

Neural circuitry of a polycystin-mediated hydrodynamic startle response for predator avoidance

Luis A Bezares-Calderón^{1,2}, Jürgen Berger², Sanja Jasek^{1,2}, Csaba Verasztó^{1,2}, Sara Mendes², Martin Gühmann², Rodrigo Almeda³, Réza Shahidi^{1,2}, Gáspár Jékely^{1,2*}

¹Living Systems Institute, University of Exeter, Exeter, United Kingdom; ²Max Planck Institute for Developmental Biology, Tübingen, Germany; ³Centre for Ocean Life, Technical University of Denmark, Denmark, Kingdom of Denmark

Abstract Startle responses triggered by aversive stimuli including predators are widespread across animals. These coordinated whole-body actions require the rapid and simultaneous activation of a large number of muscles. Here we study a startle response in a planktonic larva to understand the whole-body circuit implementation of the behaviour. Upon encountering water vibrations, larvae of the annelid *Platynereis* close their locomotor cilia and simultaneously raise the parapodia. The response is mediated by collar receptor neurons expressing the polycystins PKD1-1 and PKD2-1. CRISPR-generated *PKD1-1* and *PKD2-1* mutant larvae do not startle and fall prey to a copepod predator at a higher rate. Reconstruction of the whole-body connectome of the collar-receptor-cell circuitry revealed converging feedforward circuits to the ciliary bands and muscles. The wiring diagram suggests circuit mechanisms for the intersegmental and left-right coordination of the response. Our results reveal how polycystin-mediated mechanosensation can trigger a coordinated whole-body effector response involved in predator avoidance.

DOI: <https://doi.org/10.7554/eLife.36262.001>

*For correspondence:
g.jekely@exeter.ac.uk

Competing interests: The authors declare that no competing interests exist.

Funding: See page 23

Received: 27 February 2018

Accepted: 16 November 2018

Published: 14 December 2018

Reviewing editor: Ronald L Calabrese, Emory University, United States

© Copyright Bezares-Calderón et al. This article is distributed under the terms of the [Creative Commons Attribution License](#), which permits unrestricted use and redistribution provided that the original author and source are credited.

Introduction

Approaching predators or other threatening stimuli often elicit prey escape or startle responses characterized by rapid whole-body locomotory actions (*Bullock, 1984*). For example, crayfish escape from threatening stimuli by rapid tail flips (*Edwards et al., 1999*) and fish perform a rapid 'C-shape' body bend upon vibrational or visual stimuli (*Eaton et al., 1977*). The ubiquity and stereotypy of such responses have allowed their study in a variety of organisms, uncovering many commonalities in the underlying neuronal circuitry.

Startle responses require the simultaneous activation of a large number of muscles in a coordinated manner with a short latency (*Eaton et al., 1977*). This is often achieved by a system of giant command neurons or motoneuron such as the giant fibres in crayfish (*Wiersma and Ikeda, 1964*), the Mauthner cells (M cells) in fish and lampreys (*Korn and Faber, 2005*) or the giant motor axons in the jellyfish *Aglantha digitale* (*Roberts and Mackie, 1980*). Such giant neurons increase transmission speed and accuracy, and enable activation of the locomotor system with the least number of intervening synapses (*Bullock, 1984*).

Another common feature of startle circuits is the presence of converging neuronal pathways that activate the same effectors. This can contribute to behavioural flexibility. In crayfish, a non-giant circuitry is present that enables the animal to respond more variably to less abrupt stimuli (*Edwards et al., 1999; Kramer et al., 1981*). In fish, not only the M cell but also other descending reticulospinal neurons are required for short latency responses (*Liu and Fetcho, 1999*). Convergence

can also occur at the sensory level, as shown in fish, crayfish and *Drosophila* larvae (Lacoste et al., 2015; Ohyama et al., 2015; Zucker, 1972).

The motor programs during a startle response can also differ depending on the location of the stimulus. This is due to differences in connectivity downstream of different sensory fields. In *C. elegans* (Chalfie et al., 1985) and crayfish (Wine and Krasne, 1972), partially overlapping circuits induce forward movement upon posterior stimulation, or backward movement upon anterior stimulation. In *Drosophila* larvae, backward or forward movement depends on stimulus direction. This is achieved by an interneuron type with differential connectivity in anterior and posterior segments (Takagi et al., 2017).

Startle responses and their flexibility can best be interpreted by considering the ethological context. For example, in *C. elegans*, defects in the touch response lead to a lower escape rate from fungal predators (Maguire et al., 2011). Crayfish display giant-fibre-mediated tail flips to avoid approaching predators, but non-giant-mediated tail flips to escape following capture (Herberholz et al., 2004). Studying startle behaviours using naturalistic stimuli could thus help reveal the behavioural features that have been selected for by evolution.

Startle responses are useful models to uncover the relationship between genes, circuits and behaviour. The first organism where behavioural, genetic and whole-body connectomics analysis could be integrated was the nematode *C. elegans*. Here the study of the touch withdrawal response led to the discovery of key components of the mechanosensory cascade including the DEG/ENaC mechanotransduction channel complex MEC-4 (O'Hagan et al., 2005) (reviewed in Schafer, 2015). Genetic and cell ablation techniques, combined with the analysis of the whole-body wiring diagram (White et al., 1986) allowed the characterisation of the sensory-locomotor circuits involved in the touch withdrawal response in *C. elegans* (Chalfie et al., 1985; Piggott et al., 2011).

Multilevel studies integrating whole-body connectomics, behaviour, genetics and ethology in a larger diversity of animals will help to identify general principles of the neural control of behaviour. A broader comparative approach will also be important to understand how circuits and behaviours have evolved. Here we combine behavioural assays, calcium imaging, genetic analysis and circuit reconstructions to characterise a hydrodynamic startle response in larval *Platynereis dumerilii*, a marine annelid accessible for whole-body connectomics, genetic manipulations and behaviour analysis (Randel et al., 2015; Randel et al., 2014; Verasztó et al., 2017; Williams and Jékely, 2016; Zantke et al., 2014).

Results

A hydrodynamic startle response in *Platynereis* larvae

Nectochaete larvae of the marine annelid *Platynereis dumerilii* are planktonic and swim with beating cilia arranged into segmental bands (trochs) (Figure 1A). The larva has three main trunk segments, each with two pairs of parapodia endowed with spiny chaetae and a complex musculature (Fischer et al., 2010). Upon disturbances to the surrounding water, freely swimming larvae abruptly stop swimming, contract the body and simultaneously elevate parapodia in all segments and on both sides of the body (Figure 1B–C). This response is followed by a slower recovery phase (Figure 1—figure supplement 1, Video 1).

To characterize the kinematics of the startle response, we recorded trunk-tethered larvae at 230–350 frames per second during fictive swimming and stimulated them with a vibrating tungsten filament placed at a distance from the larvae to trigger startle responses (Figure 1D and Video 2). We visualized the water flow with fluorescent microbeads (Video 3). When we stimulated larvae from the anterior, they closed their beating cilia and elevated the parapodia. Both aspects of the response were modulated as a function of filament speed (Figure 1G). The main ciliary band (prototroch) closed in all trials except at the lowest filament speeds tested (Figure 1G). The closures extended to all locomotor ciliary bands (hereafter referred to as bodytrochs) (Video 2). Although parapodial elevation was triggered with some of the lowest filament speeds tested, it was only consistently observed above 28 $\mu\text{m}/\text{ms}$. The extent of the elevation of parapodia was dependent on the speed of the filament and displayed a bimodal distribution (Figure 1G). We split the distribution into low-angle and wide-angle elevation responses (LowE and WideE, respectively) by a cutoff obtained from adjusting the data to a finite mixture model (Figure 1E–G, Video 2). LowE responses

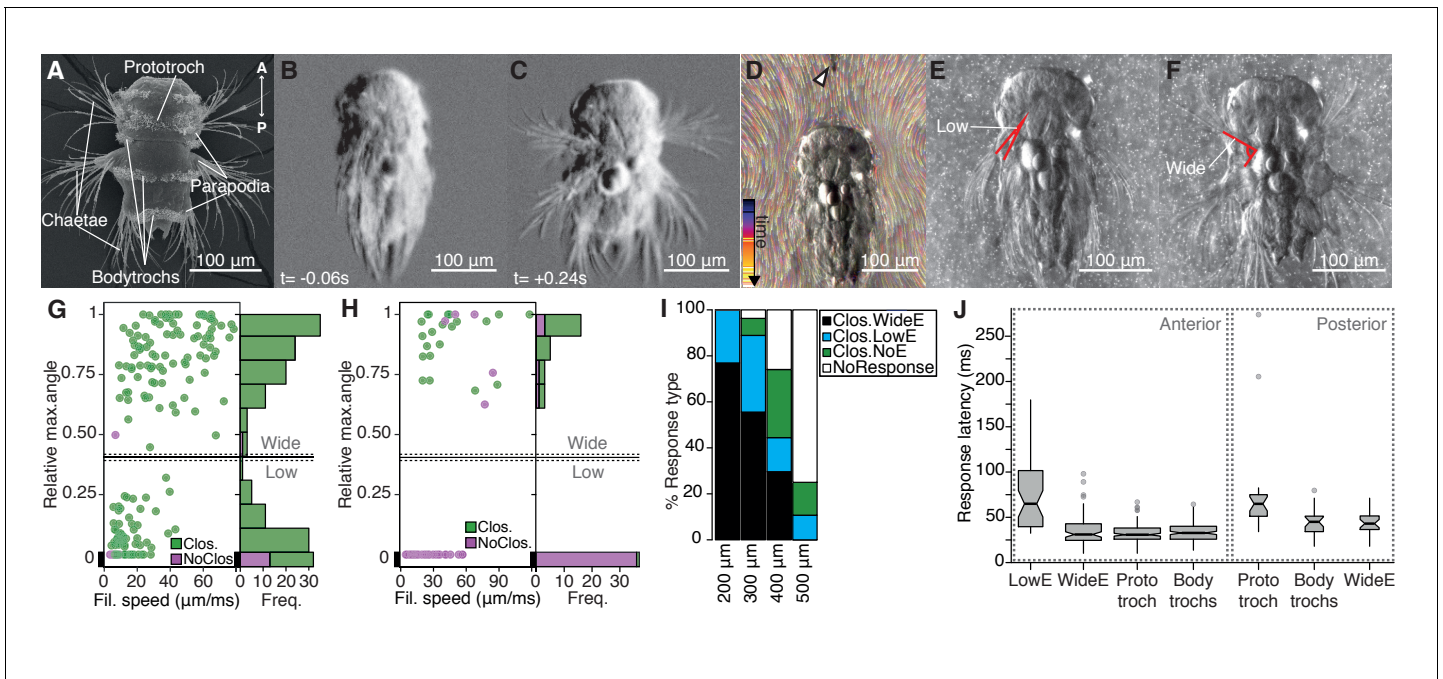


Figure 1. The startle response in *Platynereis* larvae is driven by hydrodynamic disturbances. (A) SEM micrograph of a 3-day-old nectochaete larva, dorsal view. (B–C) Snapshots of **Video 1** 60 ms before (B) and 240 ms after (C) a vibration stimulus. (D) Trunk-tethered larva (arrowhead points to the filament used for stimulation) engaging in (fictive) swimming. Fluorescent beads are colour coded by frame. (E–F) Examples of low-angle (E) or wide-angle (F) parapodial elevation upon anterior stimulation (angles measured are outlined in red). (G–H) Relative parapodial elevation angle (0, no elevation; 1, maximum elevation) as a function of filament speed. The stimulation filament was placed 100 μm from the head (G) or pygidium (H). Dots are colour coded by ciliary band (prototroch) closure. A stacked histogram is shown to the right of each scatter plot. A finite Mixture Model-based cut off (0.4, solid horizontal lines) splits the two main populations of the histogram in G. Dashed horizontal lines: 95% CI. (I) Stacked bar plot of startle response profiles upon stimulation with a filament placed at varying distances from the head. (J) Latency distributions for the onset of each response upon anterior (left) or posterior (right) stimulation. Notch in boxplots displays the 95% CI around the median. Box width proportional to \sqrt{n} . $n = 9$ larvae in panels G to J), each tested multiple times.

DOI: <https://doi.org/10.7554/eLife.36262.002>

The following source data and figure supplements are available for figure 1:

Source data 1. Source data of startle kinematics experiments.

DOI: <https://doi.org/10.7554/eLife.36262.005>

Figure supplement 1. Descriptive statistics of the startle response in freely-swimming and tethered larvae.

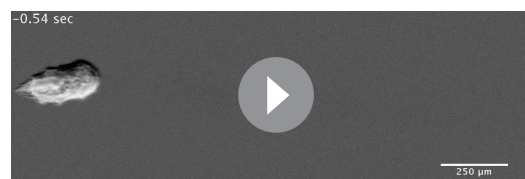
DOI: <https://doi.org/10.7554/eLife.36262.003>

Figure supplement 1—source data 1. Normalized speed and area values of startle responses in freely swimming larvae.

DOI: <https://doi.org/10.7554/eLife.36262.004>

were more common at low to moderate speeds, while WideE responses were seen across a broad stimulus-intensity spectrum (**Figure 1G**, **Figure 1—figure supplement 1**). WideE responses had a shorter latency and the maximum parapodial elevation was achieved sooner than LowE responses (**Figure 1J**, and data not shown). Ciliary arrests and WideE responses occurred in close succession to each other (**Figure 1—figure supplement 1**). As we moved the filament further away from the head, the response profile shifted to greater filament speeds (**Figure 1I**), showing that the response is triggered by near-field hydrodynamic disturbances.

Next, we stimulated larvae from the posterior end (pygidium) from a 100 μm distance. Posterior stimulation triggered startle behaviours with a markedly different response profile compared



Video 1. Startle response of *Platynereis* larvae. Time relative to start of stimulus.

DOI: <https://doi.org/10.7554/eLife.36262.006>

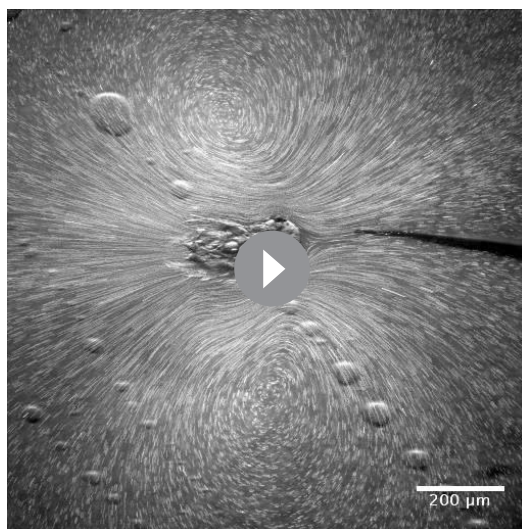


Video 2. Graded startle responses of a glued *Platynereis* larva stimulated with a vibrating filament. Low stimulus intensity triggers ciliary closures only (as assessed by stop of the fluorescent beads around the larva), intermediate stimulation induces ciliary closures and low-angle parapodial elevation, and high intensity stimulation induces ciliary closures and wide-angle parapodial elevation (WideE). Time is relative to stimulus start.

DOI: <https://doi.org/10.7554/eLife.36262.007>

the onset of elevation of the first pair of left and right parapodia were mostly below our recording speed limit (**Figure 1—figure supplement 1**). Parapodia in different segments, but on the same body side rose simultaneously or one frame apart from each other (**Figure 1—figure supplement 1**).

We thus characterized a rapid, left-right symmetric, segmentally coordinated, stereotypical whole-body startle response. The response is triggered by hydrodynamic stimuli and has a scalable profile that is different depending on the direction of stimulus.



Video 3. Flow field generated by beating cilia around a glued *Platynereis* larva. Fluorescent beads were added in order to visualize flow. The stimulation needle is located in front of the larva. Some drops of dried glue are visible.

DOI: <https://doi.org/10.7554/eLife.36262.008>

to anterior stimuli (**Figure 1H**). First, animals were less sensitive to posterior stimulation as only filament speeds $>19 \mu\text{m}/\text{ms}$ triggered a response. Second, we only observed WideE and no LowE responses. The WideE responses were often not accompanied by ciliary closures. On the contrary, we only very rarely observed (prototroch) ciliary closures not accompanied by a WideE response. WideE responses triggered from anterior and posterior stimulation were similarly fast (anterior and posterior WideE response median latency: 31.7 ms and 42 ms, respectively) (**Figure 1—figure supplement 1**) WideE responses accompanied by prototroch ciliary closures were temporarily uncoupled (ciliary closures median latency: 65 ms (prototroch) or 45.6 ms (bodytrochs);) (**Figure 1J, K**).

During WideE responses the three chaeta-bearing segments and the left and right body sides were highly coordinated. As already apparent from freely swimming larvae (**Figure 1C**) the extent of the elevation was bilaterally symmetric in all responses observed (**Figure 1F** shows a representative example). The delay values between

Collar-receptor neurons respond to water-borne vibrations

To understand the neuronal mechanism of the startle response, we searched for candidate mechanosensory neurons in *Platynereis* larvae. The most likely candidates to sense flow-driven strain and bending are neurons with ciliary structures penetrating the cuticular surface (**Budelmann, 1989**). Using a combination of scanning (SEM) and ssTEM, we identified and mapped all penetrating unciliated, biciliated and multiciliated sensory neurons across the whole body of nectochaete larvae (**Figure 2** and **Figure 2—figure supplement 1**). Since nectochaete larvae have a stereotypical morphology, the same cells could be reliably identified in different larvae by SEM and in the ssTEM dataset (**Randel et al., 2015**).

We focused on penetrating ciliated sensory neurons on the head of the animal, as this region was the most sensitive to mechanosensory stimuli (**Figure 1**). We found different candidate cell types (**Figure 2A–B**), including a group of cells very similar to the collar receptor cells (CRs)

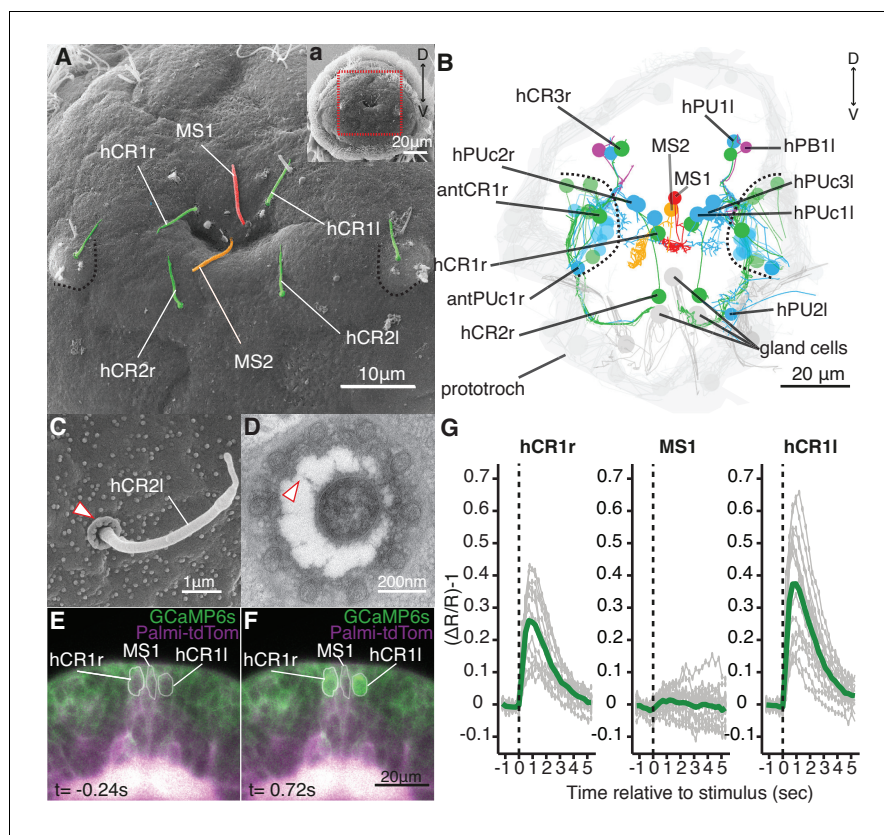


Figure 2. Head CR neurons are hydrodynamic receptors. (A) Close-up view of the head of a nectochaete larva (region outlined in a). Developing antennae with a CR cilium (green) are outlined in blue. (B) Reconstruction of penetrating ciliated sensory neurons in the head from a serial transmission electron microscopy volume. Colour code as in (A). Additional penetrating unciliated (PUc and PU) or biciliated (PB) neurons are shown in blue and magenta, respectively. One of each bilateral pair is labelled. Cells not fully penetrating the cuticle are shown in semi-transparent colors. (C) SEM of a CR sensory cilium (hCR2l), collar of microvilli protrudes out of the cuticle (arrowhead). (D) TEM cross-section of a CR sensory cilium with a collar of 10 thick microvilli and fibres connecting the cilium and the microvilli (arrowhead). (E, F) Snapshots from **Video 5** showing a larva injected with *Palmi-tdTomato-P2A-GCaMP6s* mRNA 0.24 s prior (E) or 0.72 s after (F) stimulation with a vibrating filament (ventral view). The ROIs used for fluorescence quantification are outlined in white. (G) Mean ratiometric fluorescence changes (green traces) of hCR1l, hCR1r and MS1 neurons upon stimulation with a vibrating filament placed 50 μm anterior to the head. 15 (hCR1r), 18 (MS1) and 16 (hCR1l) measurements (grey traces) from five animals are shown. The traces were aligned relative to the stimulus start ($t = 0$).

DOI: <https://doi.org/10.7554/eLife.36262.009>

The following source data and figure supplements are available for figure 2:

Source data 1. Source data of calcium imaging experiments.

DOI: <https://doi.org/10.7554/eLife.36262.012>

Source data 2. Sequence and map of plasmid construct used to synthesize *Palmi-tdTomato-P2A-GCaMP6s* mRNA.

DOI: <https://doi.org/10.7554/eLife.36262.013>

Figure supplement 1. Penetrating ciliated sensory neurons in the nectochaete larva.

DOI: <https://doi.org/10.7554/eLife.36262.010>

Figure supplement 2. Distinct head CR and MS neurons are identifiable in living animals.

DOI: <https://doi.org/10.7554/eLife.36262.011>

previously identified in other polychaetes (*Budelmann, 1989; Purschke, 2005; Purschke et al., 2017; Schlawny et al., 1991; Windoffer and Westheide, 1988*), earthworms (*Knapp and Mill, 1971*) and leeches (*Phillips and Friesen, 1982*). The CR neurons in *Platynereis* have a single non-motile cilium with a $9 \times 2 + 2$ microtubule doublet pattern and a symmetric collar of 10 thick microvilli surrounding the cilium (**Figure 2C–D**). Each microvillus has a dense region in the inner side and

is connected by thin fibres to the cilium (**Figure 2D**). The collar and the cilium penetrate the cuticle, thus these cells can also be identified in SEM samples (**Figure 2C**). CR neurons also occur in other regions of the nectochaete larva, either individually or in clusters as parts of developing organs (**Figure 2A,B**, and **Figure 2—figure supplement 1**).

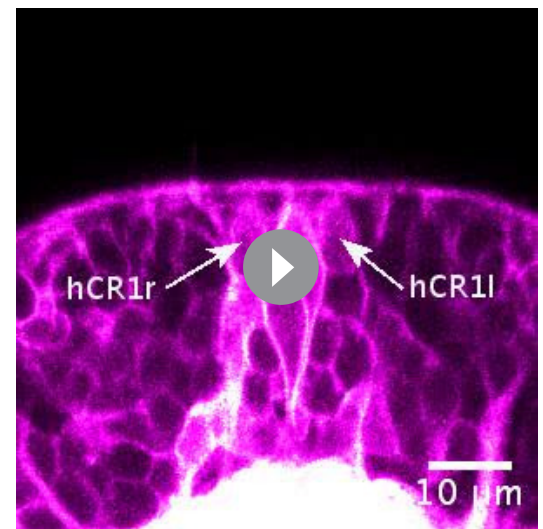
To determine if the head CR neurons are hydrodynamic mechanoreceptors, we recorded the activity of a set of clearly identifiable head CR neurons (hCR1 and hCR2) by calcium imaging (**Figure 2E**, **Figure 2—figure supplement 2** and **Video 4**). We also imaged another distinct type of collared unciliated penetrating neuron called MS1 located between the two hCR1 cells (**Figure 2A–B** and **Figure 2—figure supplement 2**). The cell bodies of hCR1 and MS1 neurons lie in the same focal plane and could be recorded simultaneously (**Figure 2E,F**, **Figure 2—figure supplement 2**). When we stimulated larvae with a vibrating filament, the cilia of the hCR1 cells deflected and GCaMP6s fluorescence increased in the cell bodies and in the cilia (**Figure 2E–G**, **Video 5** and **Video 6**). Although the cilium of MS1 was also deflected, the fluorescence did not increase in this cell (**Figure 2G**, and **Video 6**). hCR2 neurons were also activated by the stimulus (**Figure 2—figure supplement 2**). These results show that head CR neurons detect hydrodynamic vibrations and could thus trigger the startle response.

CR neurons express polycystin channels

To investigate the mechanism of hydrodynamic reception, we searched for mechanosensory markers specifically expressed in CR neurons. We found that a *Platynereis* ortholog of the TRPP/Polycystin-2 channel, *PKD2-1*, (**Figure 3—figure supplement 1**) was expressed in CR neurons, as demonstrated by *in situ* hybridization and a transgenic reporter construct (**Figure 3A,B,D**). *PKD2-1* was also expressed in two other types of penetrating uni- and biciliated sensory neurons (PU and PB neurons, respectively) in the head, trunk, and pygidium, including an unpaired biciliated sensory cell in the pygidium (pygPB^{unp}) (formerly pygPB^{bicil}; **Shahidi et al., 2015**; **Verasztó et al., 2017**) (**Figure 3—figure supplement 2**). Another gene in *Platynereis*, *PKD1-1*, was expressed only in CR neurons and in the pygPB^{unp} neuron at the nectochaete stage (**Figure 3A,C,E** and **Figure 3—figure supplement 3** and **Video 7**). *PKD1-1* belongs to the TRPP-related family PKD1, and it defines a novel invertebrate family that is paralogous to the more widespread Polycystin-1 and PKD1L1 families (**Figure 3—figure supplement 1**).

PKD1-1 and PKD2-1 are required for the startle response

The co-expression of *PKD1-1* and *PKD2-1* in CR neurons and the known function of their homologs in mechanotransduction (**Nauli et al., 2003**; **Sharif-Naeini et al., 2009**) suggested that polycystins participate in the mechanotransduction cascade in CR neurons. To test this, we generated mutant lines with the CRISPR/Cas-9 system (**Lin et al., 2014**). We recovered multiple deletion alleles in both *PKD1-1* and *PKD2-1* with frameshift mutations and premature STOP codons leading to protein products predicted to lack most functional domains (**Figure 4A–D**). Homozygote and trans-heterozygote larvae for either *PKD1-1* or *PKD2-1* alleles were viable and fertile and had normal CR neuron morphology (**Figure 4—figure supplement 1**). These larvae, however, failed to startle upon touching their head, a stimulus that triggered the startle response in most wild type and heterozygote larvae (**Figure 4E–F**, **Figure 4—source data 1**). We also tested the responses of tethered *PKD1-1* and *PKD2-1* mutant larvae stimulated from the anterior or the posterior end with a vibrating filament (**Figure 4G–H**, **Video 8**, **Figure 4—source**



Video 4. Morphology of the hCR1 neurons marked with Palmi-tdTomato. Circles track the dendrite projection towards the cilia of each hCR1.

DOI: <https://doi.org/10.7554/eLife.36262.014>

data 2). All aspects of the startle response, including ciliary arrests and parapodial extensions were absent from mutant larvae for either of the genes across the whole range of filament speeds tested. This demonstrates that the neuronal expression of *PKD1-1* and *PKD2-1* channels is essential for the hydrodynamic startle response in *Platynereis* larvae.

The absence of a startle response in the otherwise normal polycystin mutants allowed us to test whether the startle response plays a role in prey-predator interactions, as suggested for other planktonic larvae that have a similar response (Pennington and CHIA, 1984; Thiel et al., 2017). We exposed *Platynereis* larvae to *Centropages typicus*, a predatory copepod which detects its prey by the hydromechanical signals generated by prey locomotion (Calbet et al., 2007; Cowles and Strickier, 1983; Kerfoot, 1978) (Figure 5A). We incubated in the same container an equal amount of *PKD2-1^{mut/mut}* and age-matched wildtype larvae with *C. typicus* and quantified the number of survivors of each genotype after 12 hr or 24 hr. We also incubated larvae without copepods to control for differences in mortality rates not related to predation (Figure 5—source data 1). In most experiments, *PKD2-1^{mut/mut}* larvae were predated more than their wildtype counterparts ($p < 0.001$, one-sided exact Wilcoxon-Pratt signed rank test, Figure 5B). As wild type but not mutant larvae showed the startle response upon copepod attacks (Video 9), the difference in predation rates is likely due to the absence of a startle response in *PKD2-1^{mut/mut}* larvae.

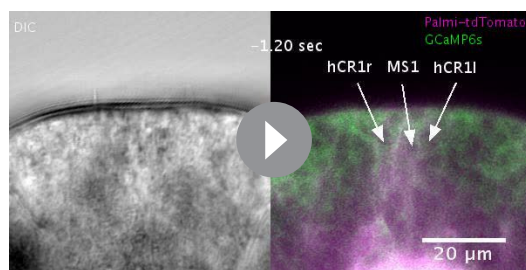
Whole-body wiring diagram of the startle response

The hydrodynamic sensitivity of the head CR neurons (Figure 2), their expression of PKD genes (Figure 3), and the requirement of these genes for the startle response (Figure 4) argue for the CRs as the main sensory receptors that trigger the startle response. To investigate the neuronal mechanisms behind the response, we mapped the wiring diagram of chemical synapses downstream of all CRs in a whole-body ssTEM dataset (Randel et al., 2015). We identified all the direct postsynaptic partners (more than two synapses from more than 1 CRs) of CRs in the larva (Figure 6—source data 1–2, Video 10). We only analysed the most direct neural paths from CRs to the ciliated and muscle effectors, assuming the initiation of the response here described would use the path with the fewest intervening synapses. The head and pygidial CRs project along the ventral nerve cord (VNC) posteriorly and anteriorly, respectively (Figure 6A and Figure 6—figure supplement 1), and form *en passant* synapses with distinct types of interneurons (INs) and motoneurons (MNs) (Figure 6B–F, Figure 6—figure supplement 1). These INs in turn target muscle-motor and ciliomotor neurons that innervate several muscle types and the ciliary bands in the larva on both body sides (Figures 6–8).

The head CRs directly synapse on the MC cell, a previously described cholinergic motoneuron that induces ciliary closures of the prototroch ciliary band (Verasztó et al., 2017) (Figure 6B). The head but not the pygidial CRs also synapse extensively on CM interneurons (IN^{CM}), a bilateral pair of ipsilaterally projecting pseudo-unipolar neurons with a soma in the 1st segment (Figure 6B–C). The CMs are presynaptic to the Loop neurons on the same side and to MN^{ant} on both body sides (Figure 6B and Figure 8). Loop and MN^{ant} are ciliomotor neurons that likely control the closures of prototroch and bodytroch cilia (Verasztó et al., 2017)(Figure 6B). Head CRs also synapse on a novel interneuron type, the Rope interneurons (IN^{rope}). These neurons have their soma in the head and have ipsilateral descending projections that span the entire VNC (Figure 6C). IN^{rope} neurons make synaptic contacts with the Loop neurons (Figure 6B), thus providing a converging pathway to ciliary control. Finally, both head and pygidial CRs target the sensory-motor neuron pygPB^{unp}, which may modulate the prototroch ciliary band system (Verasztó et al., 2017).

CRs also feed into distinct muscle-motor pathways (Figure 6B). Both head and pygidial CRs directly synapse on the Crab motoneurons (MN^{crab}), a unique set of decussating VNC motoneurons that innervate a variety of trunk muscles (Figure 6B, Figure 6—figure supplements 1 and 2). A second pathway is through the IN^{rope} interneurons (Figure 6B). The descending projections of Rope neurons target several segmentally arranged ipsi- and contralaterally projecting VNC motoneurons (MN^{vnc}) that innervate distinct sets of somatic muscles (longitudinal, oblique, transverse, and parapodial groups) in all three segments and on both body sides (Figure 7A–C, Figure 8, Figure 6—figure supplements 1 and 2).

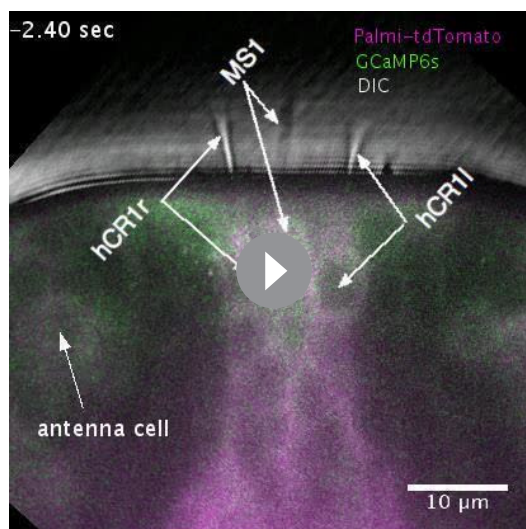
An alternative muscle-motor pathway is through the Split interneurons (IN^{split}), a group of segmentally arranged ipsilateral pseudounipolar cells (similar in morphology to CMs) (Figure 6D and Figure 6—figure supplement 1, Video 10). IN^{split} neurons synapse onto numerous ipsi- and contralaterally projecting MN^{vnc} neurons in all segments (Figure 7A and Figure 8), some of these MNs are



Video 5. Calcium imaging from the hCR1 and MS1 neurons during a vibrational stimulation. The larva is ubiquitously expressing Palmi-tdTomato and GCaMP6s. Time is relative to stimulus start.
DOI: <https://doi.org/10.7554/eLife.36262.015>

The VNC motoneurons targeted by IN^{split} , IN^{rope} and IN^{comm} belong to at least ten morphologically distinct groups, with segmentally iterated and left-right symmetric members (**Figure 7A,B, Figure 8, Figure 6—figure supplement 2**). The contralateral motoneurons MN^{crab} , MN^{ring} , MN^{spider} and MN^{smile} innervate all the distinct muscle classes involved in the startle response (longitudinal, oblique, transverse, axochord and parapodial groups) and account for most of the synaptic targets on muscles. Ipsilateral neurons target exclusively oblique and parapodial muscles (**Figure 8, Figure 6—figure supplement 2**). This is also true for MN^{bow} , a motoneuron class with both ipsilateral and decussating axonal projections (**Figure 6—figure supplement 2**). By calcium imaging during startle responses, we could directly confirm the contraction of the longitudinal, oblique, axochord and parapodial muscle groups (**Figure 7C and Video 11**).

Discussion



Video 6. Calcium imaging from the hCR1 and MS1 neurons during a vibrational stimulation. The stimulation filament and the deflection of the sensory cilia are visible. The larva is ubiquitously expressing Palmi-tdTomato and GCaMP6s.
DOI: <https://doi.org/10.7554/eLife.36262.016>

also targeted by IN^{rope} (see Venn diagram in **Figure 7A; Figure 6—figure supplement 2A**). IN^{split} cells are postsynaptic to head, trunk and pygidial CRs (**Figure 6B**).

CRs also synapse on a heterogenous group of ascending and descending trunk commissural interneurons (IN^{comm}) (**Figure 6E and Figure 6—figure supplement 1**). In contrast to the other interneuron types, we could not find bilateral pairs of IN^{comm} targeted by left and right CRs (**Figure 6—figure supplement 1**). Some of these commissural neurons synapse on contralateral interneurons and motoneurons in the startle network and also feed back to the CRs (**Figure 6B and Figure 8**). The majority of motoneurons targeted by IN^{comm} are also targeted by IN^{split} and IN^{rope} (see Venn diagram in **Figure 7A**).

Collar receptor neurons mediate a hydrodynamic startle response in *Platynereis* larvae

In this study, we described a startle behaviour in the planktonic *Platynereis* larva triggered by hydrodynamic disturbances. We identified a group of mechanosensory neurons, the CRs, that respond to hydrodynamic stimuli and express the polycystin homologs *PKD1-1* and *PKD2-1*. Through CRISPR mutagenesis, we showed that the startle response requires both *PKD1-1* and *PKD2-1*. We also provided evidence for the importance of *PKD2-1* in escaping a rheotactic predator. Connectomic analysis of the CR sensory-motor circuit identified distinct circuit motifs that could explain the whole-body temporal and spatial coordination characteristic of the startle behaviour (**Figure 8; Supplementary file 1**).

We identified the CR neurons as the hydrodynamic mechanosensory receptors initiating the startle response. CRs have a sensory dendrite with a cilium and a collar of microvilli, an arrangement commonly found in mechanoreceptors in other annelids (**Budelmann, 1989; Knapp and Mill, 1971; Phillips and Friesen,**

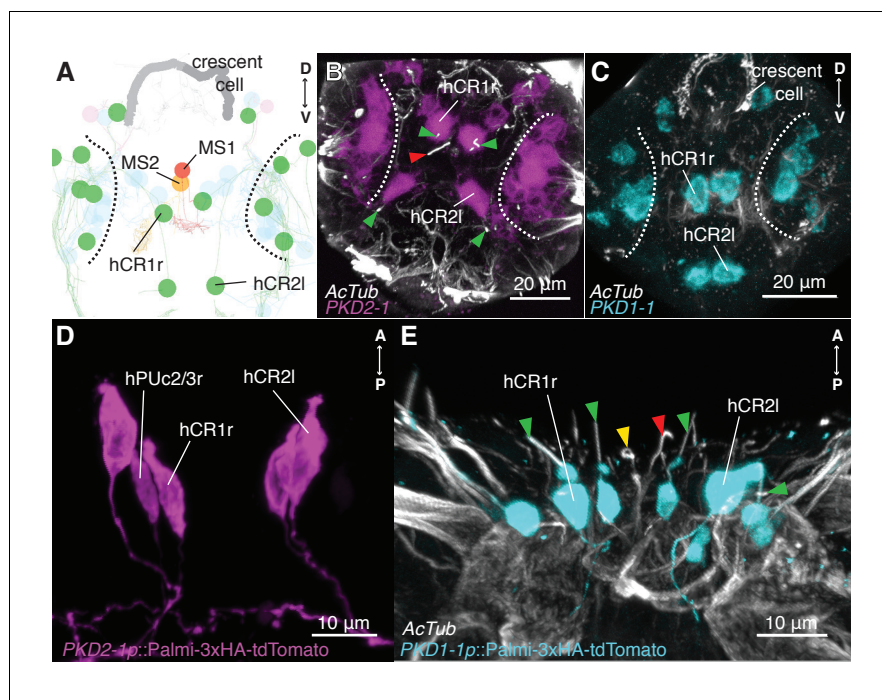


Figure 3. CR neurons express *PKD1-1* and *PKD2-1*. (A) Electron microscopy volume reconstruction of penetrating ciliated cells in the head. Only soma position of CRs (green) and MS cells are highlighted for comparison with panels B and C. Black dashed lines demarcate the antennal region. Refer to **Figure 2B** for a more detailed view. (B and C) *PKD1-1* (B) or *PKD2-1* (C) head gene expression revealed by in situ hybridization; anterior views. Compare cell position in B and C to panel A. White dashed lines demarcate the antennal region. (D and E) Immunostaining of 3xHA-Palmi-tdTomato expressed under the *PKD1-1* (D) or the *PKD2-1* (E) promoter; ventral views. Counterstaining against acetylated tubulin (AcTub) is in white. Green arrowheads in C and D point to CR cilia (green), MS1 (red) or MS2 cilia (yellow).

DOI: <https://doi.org/10.7554/eLife.36262.017>

The following source data and figure supplements are available for figure 3:

Figure supplement 1. *Platynereis* PKD1-1 and PKD2-1 belong to the TRPP/PKD1 superfamily.

DOI: <https://doi.org/10.7554/eLife.36262.018>

Figure supplement 1—source data 1. Source data of phylogenetic analysis, including alignment and tree files and nucleotide sequences of all *Platynereis* PKD genes analysed.

DOI: <https://doi.org/10.7554/eLife.36262.019>

Figure supplement 2. *PKD2-1* is expressed in CR and other penetrating ciliated neurons.

DOI: <https://doi.org/10.7554/eLife.36262.020>

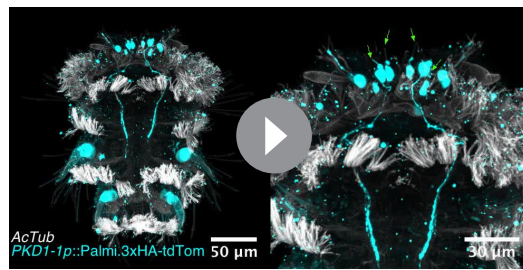
Figure supplement 3. *PKD1-1* is expressed in CR and pygPB^{unp} neurons.

DOI: <https://doi.org/10.7554/eLife.36262.021>

1982; Purschke et al., 2017; Schlawny et al., 1991; Windoffer and Westheide, 1988). In leeches, these cells (called 'S hairs') were suggested to be involved in the detection of water movement (Friesen, 1981). Morphologically, CR neurons are also similar to hair cells in vertebrates, which also can detect water movement (Engelmann et al., 2000). Further comparative work is needed to clarify the evolutionary relationships of these mechanosensory cell types (Fritzsch et al., 2007).

A neuronal function of polycystins in *Platynereis* mechanosensation

At the molecular level, we uncovered an essential function of PKD1-1 and PKD2-1 in the transduction of hydrodynamic signals by CR neurons. The role of polycystins (for the phylogeny, see **Figure 3—figure supplement 1**) in neuronal mechanotransduction is poorly understood. Most studies focused on their functions in flow detection in endothelial cells in the kidney (Nauli et al., 2008; Nauli et al., 2003; Pazour et al., 2002; Yoder et al., 2002) and in nodal cilia during embryonic development (Yoshida et al., 2012). In mammalian hair cells, polycystin-1 (PC1), a paralog of *Platynereis* PKD1-1,



Video 7. Immunostained nectochaete larva against 3xHA-Palmi-tdTomato expressed under the *PKD1-1* promoter (*PKD1-1p::Palmi-3xHA-tdTom*) and counterstained against acetylated tubulin (AcTub). Right: full body view, Left: close up of the head region. Green arrows point to the hCR1 and hCR2 cilia.

DOI: <https://doi.org/10.7554/eLife.36262.022>

sensory function (Barr and Sternberg, 1999). Despite this requirement, calcium signalling is not impaired in mechanosensory neurons in the *C. elegans* *PKD2* mutant (Zhang et al., 2018). Future studies in the experimentally tractable *Platynereis* larvae, including calcium imaging in the mutants, could contribute to elucidating the role of these molecules in neuronal mechanotransduction.

Startle responses in predator avoidance by planktonic larvae

The startle response in *Platynereis* larvae consists of the fast and synchronous activation of specific muscles and the arrest of all locomotor cilia. These responses were absent in larvae mutant for *PKD1-1* and *PKD2-1*. The use of *PKD2-1* mutant larvae allowed us to test the importance of the startle response in avoiding a natural predator, the copepod *Centropages typicus*. We attributed the large increase in predation on *PKD2-1* mutants by this copepod to a defective startle response. Mechanosensation is thought to be especially important for predator-prey interactions at small scales (Andersen et al., 2016; Martens et al., 2015). *Platynereis* larvae mutant for *PKD2-1* would not stop swimming even at close distance from the copepod, which uses mechanoreceptors in its antennae to localize prey (Yen et al., 1992). The lack of chaetal elevation would also make the mutants more susceptible to a copepod attack. Since *PKD2-1* is also expressed in other sensory cell types (e.g. PB neurons), we cannot rule out that other sensory defects contributed to the vulnerability of mutant larvae. Similar experiments with larvae mutant for *PKD1-1*, a gene specifically expressed in CR neurons, will be needed to strengthen our conclusion. The detailed analysis of hydrodynamic interactions between *Centropages* and *Platynereis* larvae, combined with the use of mutant *Platynereis* larvae represent an exciting future avenue of investigations.

Potential circuit implementations of the graded and direction sensitive startle behaviour

Calcium imaging and the *PKD1-1* and *PKD2-1* mutants allowed us to link the hydrodynamic startle response to the CR neurons. By full-body electron microscopy we could then map the entire circuit downstream of CRs. The whole-body circuit reconstruction provided a framework to interpret the behaviour and propose hypotheses about how the different responses are controlled. We uncovered two major synaptic paths from CR neurons, one to ciliated effectors, and another one to a subset of somatic muscles. During the startle response, both ciliary and muscle effectors can be activated. Ciliary beating is controlled by a rhythmically activated ciliomotor system that drives alternating phases of ciliary activity and closures (Tosches et al., 2014; Verasztó et al., 2017). We propose that slight disturbances in the surrounding medium activate the CR neurons in the head of the larva to drive the closure of all locomotor cilia in a coordinated fashion. This could be driven by a feed-forward circuit from head CRs to the cholinergic MC neuron and the activation of the cholinergic Loop and MN^{ant} ciliomotor neurons via the CM interneurons. The beating of cilia generates a hydrodynamic

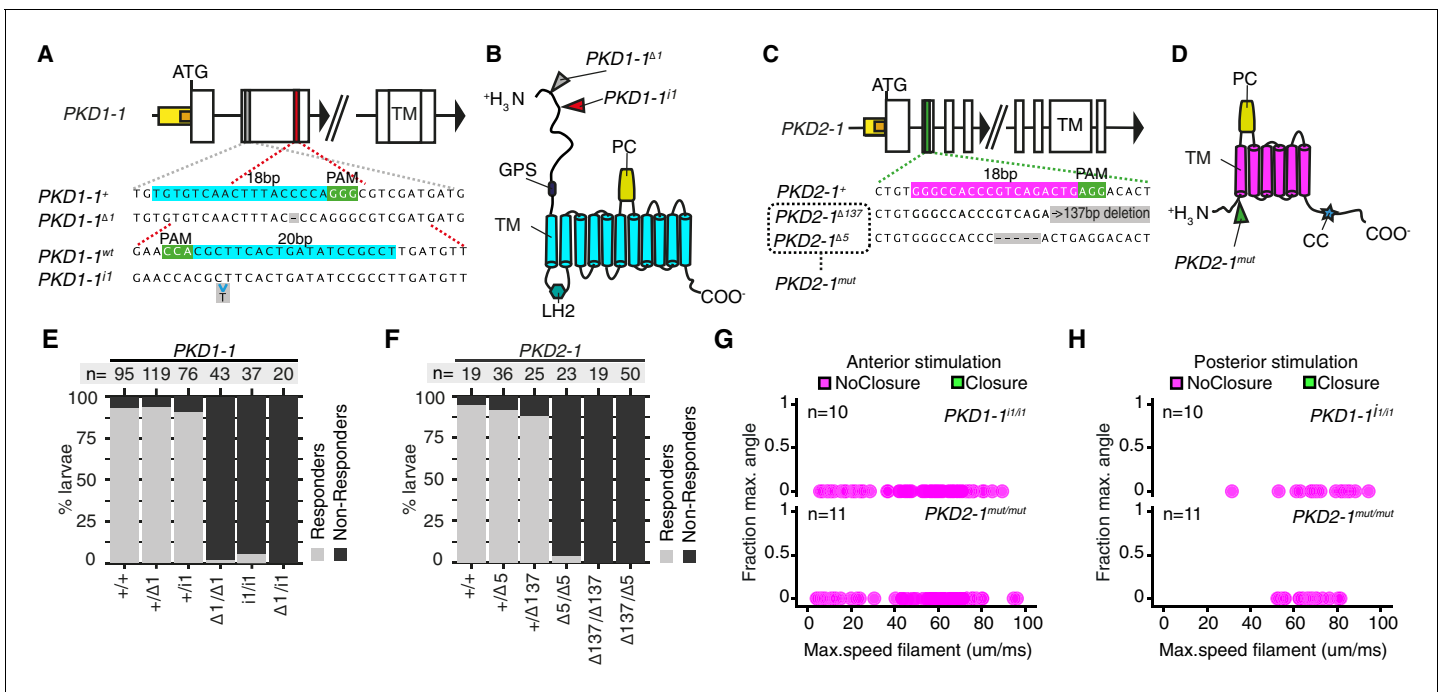


Figure 4. PKD1-1 and PKD2-1 are required for the startle response. (A and C) PKD1-1 (A) and PKD2-1 (C) genomic loci and close-up regions showing wildtype (+) sequences targeted with CRISPR/Cas9. The mutant alleles generated are also shown. White, yellow and orange boxes represent exons, promoters, and 5'UTRs, respectively. (B and D) PKD1-1 (B) or PKD2-1 (D) protein secondary structure. Main conserved domains are labelled. Mutation sites are indicated by arrowheads. (E and F) Stacked barplots of PKD1-1 (E) or PKD2-1 (F) mutant and wildtype (+/+) homozygote, heterozygote or trans-heterozygote larvae (%) startle response to touch stimulus. Data in (E) and in (F) from 18 or 14 batches, respectively. (G and H) Parapodial elevation angles of PKD1-1^{i1/i1} or PKD2-1^{mut/mut} larvae as a function of filament speed. Stimulation filament ca. 100 μm from anterior (G) or from posterior (H).

DOI: <https://doi.org/10.7554/eLife.36262.023>

The following source data and figure supplement are available for figure 4:

Source data 1. Phenotyping of PKD1-1 and PKD2-1 mutant larvae in the touch assay.

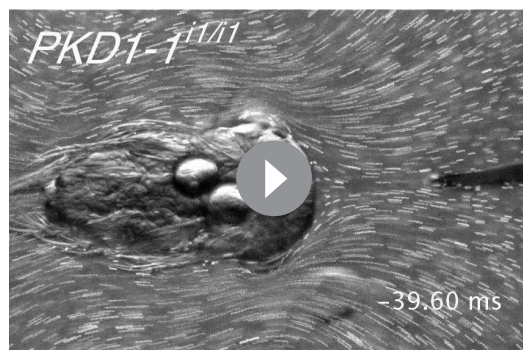
DOI: <https://doi.org/10.7554/eLife.36262.025>

Source data 2. Phenotyping of tethered PKD1-1 and PKD2-1 mutant larvae.

DOI: <https://doi.org/10.7554/eLife.36262.026>

Figure supplement 1. Cilia of hCR1 and hCR2 neurons in PKD1-1^{i1/i1} or PKD2-1^{mut/mut} larvae are morphologically similar to wildtype controls.

DOI: <https://doi.org/10.7554/eLife.36262.024>



Video 8. No startle response in a PKD1-1^{i1/i1} mutant *Platynereis* larva exposed to a high-intensity stimulus. Time is relative to stimulus start.

DOI: <https://doi.org/10.7554/eLife.36262.027>

signal that can be detected by predators at a distance (Kjørboe and Visser, 1999). By shutting off cilia upon vibrations elicited by an approaching predator, the larva could avoid being detected (Figure 9A). The ability to cease ciliary beating upon mechanical stimulation has been reported in other ciliated larvae (Mackie et al., 1976) and could be a widespread predator avoidance mechanism.

At higher stimulation intensities, we observed the rapid closure of the ciliary bands and the simultaneous wide elevation of all parapodia. This defensive behaviour could be triggered by an attacking predator (Figure 9C and Video 9). The wiring diagram suggests that Rope neurons could simultaneously activate ciliomotor and trunk musculomotor neurons across all segments

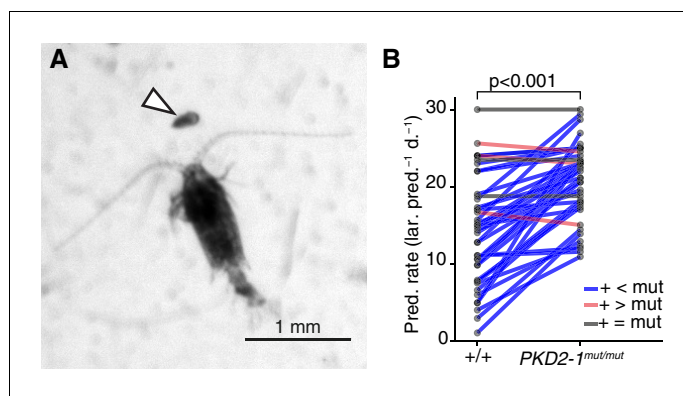


Figure 5. *PKD2-1* is required for predator avoidance and escape. (A) Adult *Centropages typicus* female approaching a nectochaete *Platynereis* larva (arrowhead). (B) Predation on wildtype (+/+) and *PKD2-1^{mut/mut}* larvae by *C. typicus*. Paired values are joined by blue, grey or red lines if predation rates were higher, equal or lower in mutant than in wildtype larvae, respectively; data from 42 trials with 12 batches. One-sided exact Wilcoxon-Pratt signed rank test, $P = 5.2e-10$.

DOI: <https://doi.org/10.7554/eLife.36262.028>

The following source data is available for figure 5:

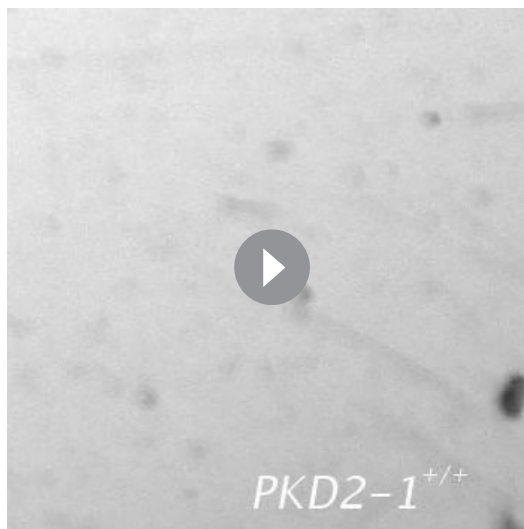
Source data 1. Source data of predation experiments.

DOI: <https://doi.org/10.7554/eLife.36262.029>

upon strong stimulation of head CRs. This could lead to the observed coordinated contraction of muscles and ciliary closures (**Figure 1J** and **Figure 1—figure supplement 1**). Thus, based on their anatomy and connectivity, Rope neurons are candidate command interneurons in *Platynereis* (**Wiersma and Ikeda, 1964**). Their circuitry resembles that of giant fibre systems in a variety of animals, such as the GF system in *Drosophila*, the lateral and medial giants in crayfish or the M cells in vertebrates (reviewed in **Hale et al., 2016**). Adult *Platynereis* worms also have a giant fibre system involved in a startle reflex (**Smith, 1957**) but how these relate to the Rope neurons is unclear.

Beside the Rope neurons, Split interneurons constitute a second pathway for synchronous and intersegmental muscle contraction (**Figure 6B**, **Figure 7A**, and **Figure 8C**). Like Rope neurons, Split neurons receive input from head CRs and target musculomotor neurons in all segments (**Figure 7A** and **Figure 6—figure supplement 2**). These two systems could function in parallel to produce the complete startle response (**Figure 9C**). A similar mechanism has been suggested to be at work during whole-body shortening in the leech. Here, the fast-conducting S-cells trigger the initial muscle contraction followed by the activation of a slower pathway mediating extensive body shortening (**Kristan et al., 2005; Shaw and Kristan, 1995**).

The Rope and Split pathways may also implement different aspects of a startle behaviour depending on context or the nature, direction or intensity of the stimulus (**Fotowat et al., 2009; Kramer et al., 1981; Liu and Fetcho, 1999**) (**Figure 8**). For example, Split but not Rope neurons are also targeted by posterior CRs. This pathway may activate muscles independent of ciliary closures, as observed upon posterior stimulation. Such a response may help the larva to deter and escape a predator approaching from the



Video 9. Copepod attack on either a wild type or a *PKD2-1^{mut/mut}* mutant *Platynereis* larva.

DOI: <https://doi.org/10.7554/eLife.36262.030>

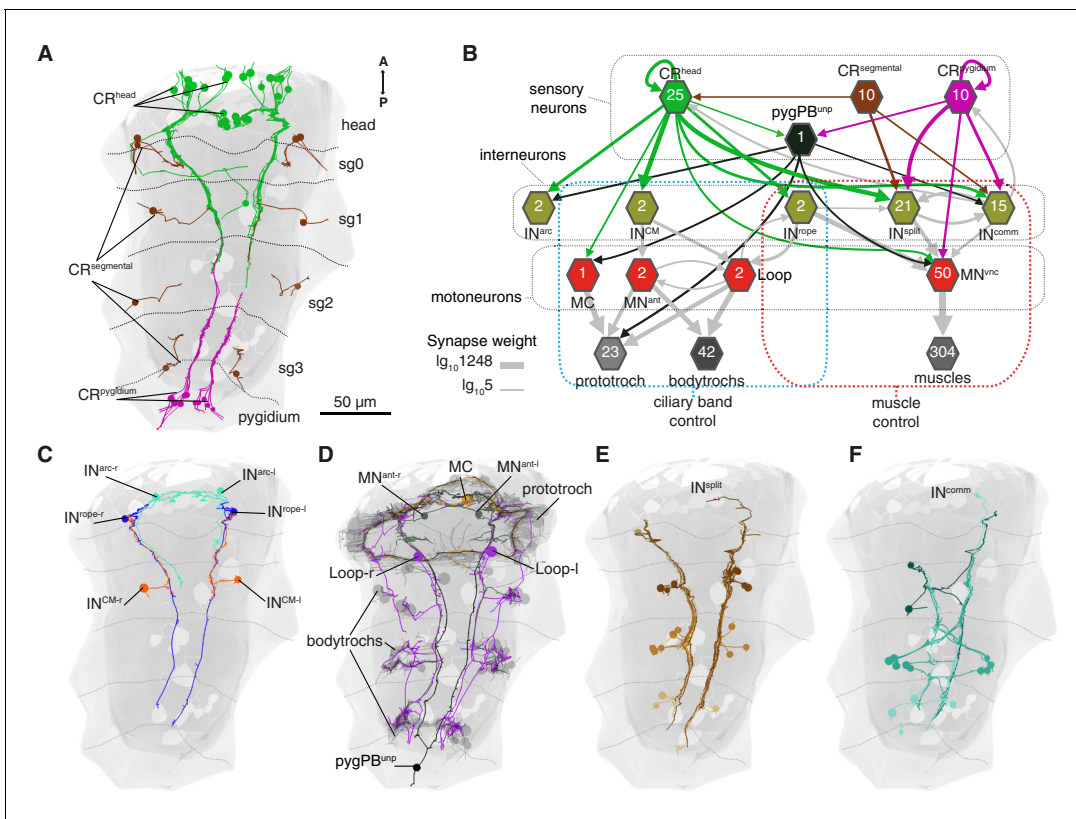


Figure 6. Wiring diagram of CR neurons. (A) All CRs in the nectochaete larva reconstructed from an EM volume. Head, segmental and pygidial groups are differently coloured. Segment (sg) boundaries are indicated by dotted lines. (B) Sensory-motor network from CR neurons to muscles and locomotory cilia. Hexagons and arrows represent neuron groups and their synaptic connections, respectively. Numbers inside hexagons indicate the number of neurons grouped in each node. Interactions with less than five synapses were filtered out in this display. Arrow line thickness (synapse weight) is equal to the common logarithm of the number of synapses (scale is shown on the bottom left of the panel). (C) EM reconstruction of IN^{rope}, IN^{arc} and IN^{CM} neurons. (D) Ciliomotor neurons targeted by CRs or by IN^{CM} (E) Ipsilateral split neurons (IN^{split}) (F) Commissural interneurons (IN^{comm}). Ventral view in A, C-F. Segment boundaries as defined in A are overlaid in C-F.

DOI: <https://doi.org/10.7554/eLife.36262.031>

The following source data and figure supplements are available for figure 6:

Source data 1. Full connectivity matrix, grouped.

DOI: <https://doi.org/10.7554/eLife.36262.035>

Source data 2. Full connectivity matrix, non-grouped.

DOI: <https://doi.org/10.7554/eLife.36262.036>

Figure supplement 1. CR neurons target ipsilateral and commissural interneurons innervating VNC motoneurons.

DOI: <https://doi.org/10.7554/eLife.36262.032>

Figure supplement 2. VNC musclemotor neuron classes in the CR neural network.

DOI: <https://doi.org/10.7554/eLife.36262.033>

Figure supplement 3. Synaptic connections in the startle circuit.

DOI: <https://doi.org/10.7554/eLife.36262.034>

posterior end (**Figure 9D**). Differences in connectivity of anterior and posterior sensory neurons to the downstream circuits have also been observed in *C. elegans* (Chalfie et al., 1985) and crayfish (Wine and Krasne, 1972). The study of the startle response in different contexts (swimming vs crawling states) combined with neuron imaging and functional interference will be needed to elucidate the contributions of these different pathways.

Bilateral coordination of the startle response

A hallmark of the startle response in *Platynereis* is its bilateral symmetry, both in timing and in the extent of muscle contraction (**Figure 1** and **Figure 1—figure supplement 1**). The proximity of the

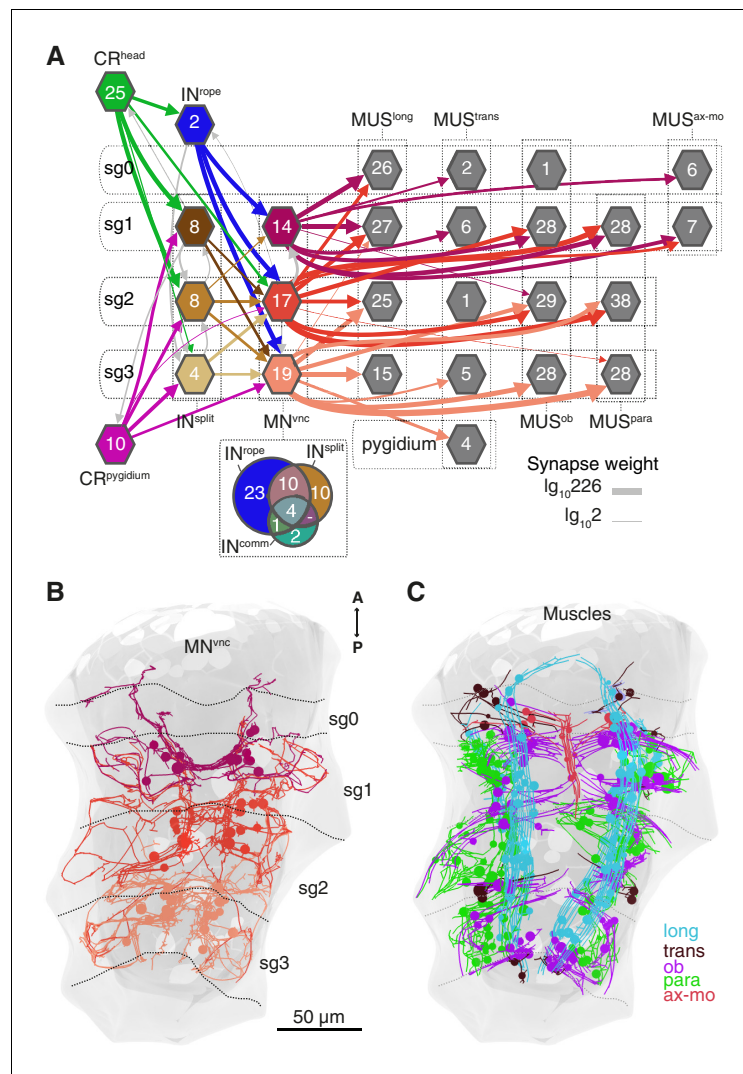


Figure 7. Segmental coordination motifs and musclemotor neuron diversity in the startle circuit. (A) Muscle network downstream of IN^{rope} and IN^{split} sorted by segmental location and muscle type. Arrows represent synaptic connections and are coloured based on the source neuronal group (represented by hexagons). Venn diagram at the bottom of the network shows the number of common or unique VNC motoneurons (MN^{vnc}) targets of IN^{rope}, IN^{split}, and IN^{comm}. (B) MN^{vnc} targeted by Rope and Split interneurons coloured by segmental location. (C) Muscles targeted by MN^{vnc} neurons coloured by type (long, longitudinal; trans, transvers; ob, oblique; para, parapodial; ax-mo, axochord-mouth). Segment (sg) boundaries are indicated by dotted lines in A and C. Arrow line thickness (synapse weight) in A is equal to the common logarithm of the number of synapses.

DOI: <https://doi.org/10.7554/eLife.36262.038>

sensory cilia of all head and pygidial CRs suggests that both the left and right members are stimulated in most cases, as observed during calcium imaging of hCR1 cells (Figure 2E–G). Since the circuitry downstream of CR neurons is bilaterally symmetric (Figure 8), a coincident activation of left and right CRs would result in a synchronous response. But even if asymmetries in CR activation occur, circuit motifs in the network could ensure the left-right coordination of muscle and ciliary effectors. Ciliary coordination may partially rely on CM interneurons targeting ciliomotor MN^{ant} cells of both body sides (Figure 8). Coincident left-right muscle contraction could be ensured by the connection of a single Rope neuron to both ipsi- and contralateral decussating motoneurons. Split neurons have a similar bilateral connectivity pattern (Figure 8). A similar network motif is present in the *Drosophila* larva, where a single commissural interneuron innervates motoneurons on both body sides (Fushiki et al., 2016). The commissural interneurons (IN^{comm}) may also contribute to left-right

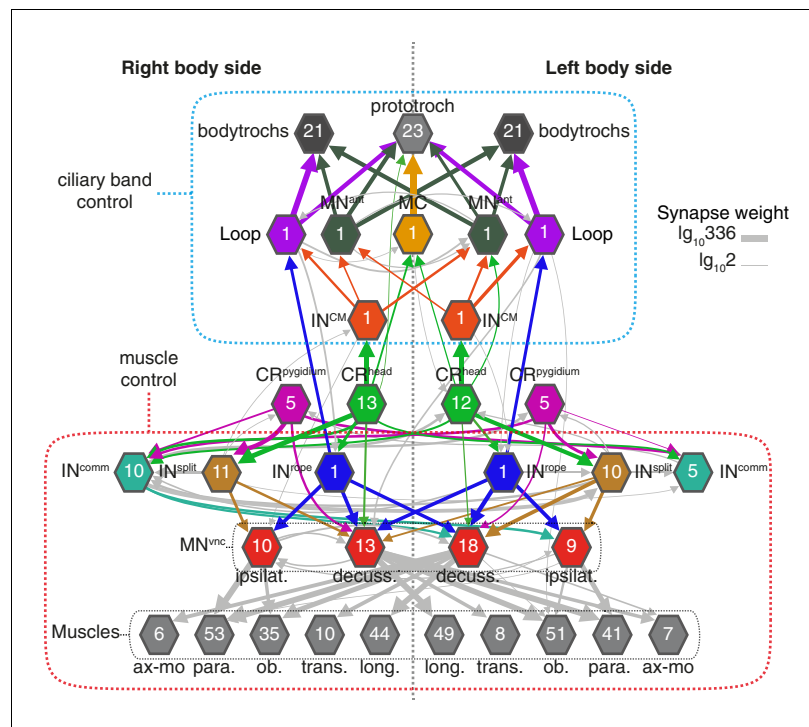
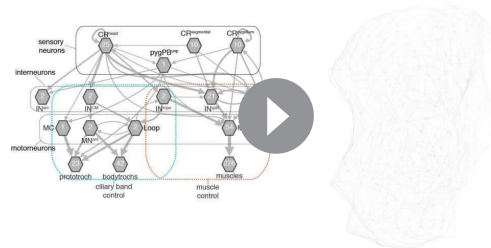


Figure 8. Bilateral coordination motifs in the startle circuit. Muscle and cilia network downstream of CR^{head} and $CR^{pygidium}$ sorted by body side. Numbers inside hexagons indicate the number of neurons grouped in each node. Interactions with less than two synapses were filtered out. Arrow line thickness (synapse weight) is equal to the common logarithm of the number of synapses.

DOI: <https://doi.org/10.7554/eLife.36262.039>

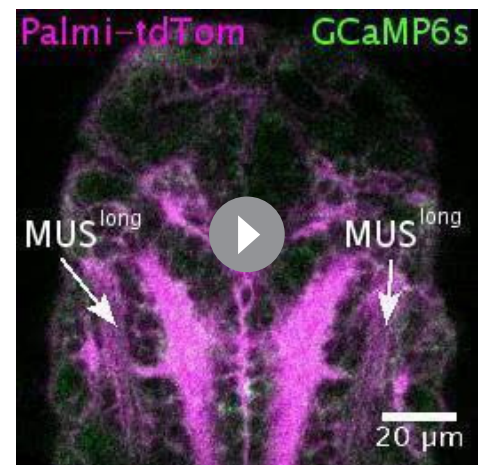
coordination. In *Drosophila*, the amplitude of muscle contractions on both body sides is controlled by ascending commissural neurons (Heckscher et al., 2015).

The study of the *Platynereis* larva allowed us to analyse in a whole-body context the molecular, cellular and circuit components of an ecologically relevant behaviour. We uncovered several motifs in this circuit that show similarities to startle circuits in other animals. The evolutionary relationship of the *Platynereis* circuit to similar circuits in



Video 10. Animation of the wiring diagram and neuronal morphology reconstructed from serial electron microscopy data. Colours in wiring diagram (left) correspond to colours of neurons in 3D model of the larva (right).

DOI: <https://doi.org/10.7554/eLife.36262.040>



Video 11. Calcium imaging from larval muscles during a startle response. The larva is ubiquitously expressing Palmi-tdTomato and GCaMP6s. The contractions of the longitudinal, oblique and parapodial muscles are visible.

DOI: <https://doi.org/10.7554/eLife.36262.041>

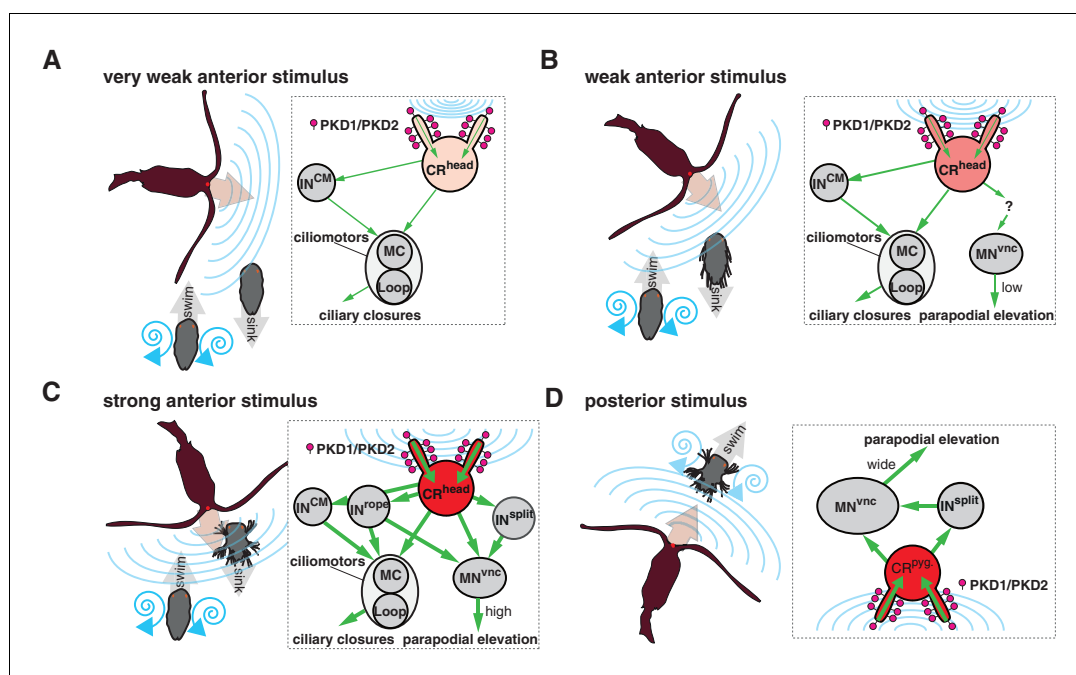


Figure 9. Summary schematics of the proposed neural implementations behind the startle response in different predator-prey scenarios. (A–D) Different interaction scenarios between a predatory copepod (brown) and a nectochaete *Platynereis* larva (grey) are schematized on the left side of each panel. Blue lines schematize hydrodynamic signals produced by the copepod or the larva. Arrows indicate the direction of movement. Inset on the right of each panel shows the proposed cellular/circuit implementation behind the corresponding larval response shown to the left. Green arrows indicate the direction of propagation of the signal. PKD1-1 and PKD2-1 (symbolized as lollipops) localize to CRs, which transduce a signal of different intensity (shown with different tones of red) depending on the strength of the hydrodynamic signal (blue lines).

DOI: <https://doi.org/10.7554/eLife.36262.042>

other bilaterians is currently unclear. Comparative connectomics of whole-body circuits has great potential to uncover circuit homologies. A recent analysis of the *Ciona intestinalis* larval connectome identified a putative startle circuit based on anatomy and connectivity alone that was suggested to be homologous to the Mauthner circuit of vertebrates (Ryan *et al.*, 2017; Ryan *et al.*, 2016). To understand circuit evolution, such approaches will need to be complemented with genetic and behavioural experiments and the analysis of the constituent cell types. Only comparisons at these different levels and at varying phylogenetic distances will allow us to reconstruct the evolution of circuits.

Materials and methods

Key resources table

Reagent type (species) or resource	Designation	Source or reference	Identifiers	Additional information
Gene (<i>Platynereis dumerilii</i>)	PKD1-1	This paper	GenBank_Acc#: MH035679	
Gene (<i>P. dumerilii</i>)	PKD2-1	This paper	GenBank_Acc#: MH035677	
Gene (<i>P. dumerilii</i>)	PKD2-2	This paper	GenBank_Acc#: MH035678	
Gene (<i>P. dumerilii</i>)	LOV-1	This paper	GenBank_Acc#: MH035680	

Continued on next page

Continued

Reagent type (species) or resource	Designation	Source or reference	Identifiers	Additional information
Strain, strain background (<i>P. dumerilii</i>)	Wild Type	Tübingen cultures, Max Planck Institute for Developmental Biology	NCBITaxon:6359	
Strain, strain background (<i>P. dumerilii</i>)	<i>PKD1-1^{Δ1/Δ1}</i>	This paper		Progenitor:Tübingen WT strain using <i>PKD1-1_truT1</i> gRNA
Strain, strain background (<i>P. dumerilii</i>)	<i>PKD1-1^{i1/i1}</i>	This paper		Progenitor:Tübingen WT strain using <i>PKD1-1_T5</i> gRNA
Strain, strain background (<i>P. dumerilii</i>)	<i>PKD2-1^{Δ137/Δ137}; PKD2-1^{mut/mut}</i>	This paper		Progenitor:Tübingen WT strain using <i>PKD2-1_truT2</i> gRNA
Strain, strain background (<i>P. dumerilii</i>)	<i>PKD2-1^{Δ5/Δ5}; PKD2-1^{mut/mut}</i>	This paper		Progenitor:Tübingen WT strain using <i>PKD2-1_truT2</i> gRNA
Strain, strain background (<i>P. dumerilii</i>)	<i>PKD2-1^{Δ137/Δ5}; PKD2-1^{mut/mut}</i>	This paper		Progenitor: <i>PKD2-1^{Δ5}</i> and <i>PKD2-1^{Δ137}</i> allele-carrying strains.
Strain, strain background (<i>Centropages typicus</i>)	Wild Type	National Institute for Aquatic Resources culture, Technical University of Denmark	NCBITaxon: 463189	
Antibody	Goat anti-Mouse IgG (H + L) Cross-Adsorbed Secondary Antibody, Alexa Fluor 488	ThermoFisher Scientific	Cat#:A11001	(1:250)
Antibody	Goat anti-Rabbit IgG (H + L) Cross-Adsorbed Secondary Antibody, Alexa Fluor 633	ThermoFisher Scientific	Cat#:A21070	(1:250)
Antibody	Monoclonal Anti-Tubulin, Acetylated antibody produced in mouse	Sigma-Aldrich	Cat#:T6793, RRID:AB_477585	(1:250)
Antibody	HA-Tag (C29F4) Rabbit mAb	Cell Signaling Technology	Cat#:3724P	(1:250)
Recombinant DNA reagent	pUC57- <i>PKD2-1p</i> ::Palmi-3xHA-tdTomato (plasmid)	This paper		Promoter construct: injected at 250 ng/μl
Recombinant DNA reagent	pUC57- <i>PKD1-1p</i> ::Palmi-3xHA-tdTomato (plasmid)	This paper		Promoter construct: injected at 250 ng/μl
Recombinant DNA reagent	pUC57-T7-RPP2-tdTomato-P2A-GCaMP6 (plasmid)	This paper		Used for generating tdTomato-P2A-GCaMP6s mRNA
Recombinant DNA reagent	pMJ920 (plasmid)	DOI: 10.7554/eLife.00471	Addgene_plasmid: #42234	Laboratory of Jennifer Doudna
Recombinant DNA reagent	pUC57-T7-RPP2-hSpCas9-HA-2XNLS-GFP (plasmid)	This paper		Used for generating Cas9-GFP mRNA
Recombinant DNA reagent	pGP-CMV-GCaMP6s (plasmid)	DOI: 10.1038/nature12354	Addgene_plasmid: #40753	Laboratory of Douglas Kim
Recombinant DNA reagent	pX335-U6-Chimeric_BB-CBh-hSpCas9n(D10A) (plasmid)	DOI: 10.1126/science.1231143	Addgene_plasmid: #42335	Laboratory of Feng Zhang
Recombinant DNA reagent	DR274 (plasmid)	DOI: 10.1038/nbt.2501	Addgene_plasmid: #42250	Laboratory of Keith Joung
Recombinant DNA reagent	<i>PKD2-1_truT2</i> (plasmid)	This paper		Derived from Addgene plasmid 42250.Used for gRNA synthesis

Continued on next page

Continued

Reagent type (species) or resource	Designation	Source or reference	Identifiers	Additional information
Recombinant DNA reagent	<i>PKD1-1_truT1</i> (plasmid)	This paper		Derived from Addgene plasmid 42335.Used for gRNA synthesis
Recombinant DNA reagent	<i>PKD1-1_T5</i> (plasmid)	This paper		Derived from Addgene plasmid 42335.Used for gRNA synthesis
Recombinant DNA reagent	pCR11- <i>PKD2-1</i> (plasmid)	This paper		Used for synthesizing WMISH probes
Recombinant DNA reagent	pCR11- <i>PKD1-1</i> (plasmid)	This paper		Used for synthesizing WMISH probes
Sequence-based reagent	<i>PKD1-1</i> -WMISH forward primer (5' > 3')	This paper		TGTCCTTTGTAAGTGGTCTGGT
Sequence-based reagent	<i>PKD1-1</i> -WMISH reverse primer (5' > 3')	This paper		ATGTTCTCAGAGATTCCTTCATC
Sequence-based reagent	<i>PKD2-1</i> WMISH forward primer (5' > 3')	This paper		TCCTCGTCATCATAATATCCATTG
Sequence-based reagent	<i>PKD2-1</i> WMISH reverse primer (5' > 3')	This paper		CTCTCTTTGTTGAGTTGGTCTTT
Sequence-based reagent	<i>PKD1-1 T5</i> (gRNA)	This paper		20 ng/μl; AGGCGGATATCAGTGAAGCG; It generated i1 allele in <i>PKD1-1</i> .
Sequence-based reagent	<i>PKD1-1 truT1</i> (gRNA)	This paper		20 ng/μl; TGTGTCAACTTTACCCCA. It generated Δ1 allele in <i>PKD1-1</i> .
Sequence-based reagent	<i>PKD2-1 truT2</i> (gRNA)	This paper		20 ng/μl; GGGCCACCCGTCAGACTG. It generated Δ137 and Δ5 alleles in <i>PKD2-1</i> .
Sequence-based reagent	<i>PKD1-1_Genotyping-truT1andT5-forward primer</i> (5' > 3')	This paper		TCAAACCTGGTCAAGATTAATTCAGA
Sequence-based reagent	<i>PKD1-1_Genotyping-truT1andT5-reverse primer</i> (5' > 3')	This paper		TCTATTTCACTAATGTTGTTCTGATG
Sequence-based reagent	<i>PKD1-1 truT1-sequencing primer</i> (5' > 3')	This paper		TAAGTGAAGGTCACATACTCGTCAGT
Sequence-based reagent	<i>PKD1-1 T5-sequencing primer</i> (5' > 3')	This paper		TATGAGACTGAATGCACAATAGAGTTT
Sequence-based reagent	<i>PKD2-1_Genotyping-truT2-forward primer</i> (5' > 3')	This paper		CCCTTTGTGAGCAGGAGATGCCCTGC
Sequence-based reagent	<i>PKD2-1_Genotyping-truT2-reverse primer</i> (5' > 3')	This paper		CATGACCTGAGTGTAGTAGTACATGGT
Sequence-based reagent	<i>PKD2-1 truT2-sequencing primer</i> (5' > 3')	This paper		AACCTTCAAATATGTTCACTACAATCC
Sequence-based reagent	BamHI- <i>PKD1-1</i> promoter forward primer (5' > 3')	This paper		ATGGATCCGGAAGCCTGATAA CAAAGTGAGTAGGAA
Sequence-based reagent	Ascl- <i>PKD1-1</i> promoter reverse primer (5' > 3')	This paper		AAGGCGCGCCGCTCCTCCTCCA AGTGGCTCTACCATCTCCGTCTGTATC
Sequence-based reagent	BamHI- <i>PKD1-1</i> promoter forward primer (5' > 3')	This paper		ATGGATCCAATAAAATTTGAAC CGAGGCCAATGGA
Sequence-based reagent	Ascl- <i>PKD1-1</i> promoter reverse primer (5' > 3')	This paper		AAGGCGCGCCGCTCCTCCTCCGGG GCGTGACATCAGCCAGTAGTTGGT
Commercial assay or kit	QuickExtract	Epicentre,US	Cat#:QE09050	

Continued on next page

Continued

Reagent type (species) or resource	Designation	Source or reference	Identifiers	Additional information
Commercial assay or kit	MEGAscript T7 Transcription Kit	Ambion, ThermoFisher Scientific	Cat#:AM1354	
Commercial assay or kit	mMESSAGE mMACHINE T7 ULTRA Transcription Kit	Ambion, ThermoFisher Scientific	Cat#:AM1345	
Commercial assay or kit	MEGAclean Transcription Clean-Up Kit	Ambion, ThermoFisher Scientific	Cat#:AM1908	
Chemical compound, drug	Mecamylamine	Sigma-Aldrich	Cat#:M9020	500 μ M
Software, algorithm	Fiji	NIH	RRID:SCR_002285	
Software, algorithm	R Project for Statistical Computing	R Foundation	RRID:SCR_001905	
Software, algorithm	Imaris Version 8.0.0	Bitplane, UK.	RRID:SCR_007370	
Software, algorithm	CATMAID	DOI: 10.1093/bioinformatics/btp266	RRID:SCR_006278	
Software, algorithm	PhyML	DOI: 10.1093/sysbio/syq010	RRID:SCR_014629	
Software, algorithm	Gblocks	DOI: 10.1080/10635150701472164	RRID:SCR_015945	
Other	Wormglu	GluStitch Inc.		
Other	Fluoresbrite Multifluorescent Microspheres 1.00 μ m	Polysciences Inc, US	Cat#:24062-5	(1:1000)

Animal culture and behavioural experiments

Platynereis dumerilii wild type (Tübingen, NCBITaxon:6359) strain and the mutant lines derived from it were cultured in the laboratory as previously described (**Fischer and Dorresteijn, 2004**). The neotochaete larval stage (approximately 72 hr post fertilization) was utilized for all experiments and raised at 18°C on a 16:8 hr light/dark cycle in glass beakers. Filtered natural sea water (fNSW) was used for all the experiments.

Adult stages of the marine planktonic copepod *Centropages typicus* were used as rheotactic predators for wild type and *PKD2-1* mutant larvae. Copepods were supplied from a continuous culture at the National Institute for Aquatic Resources (Technical University of Denmark, DTU). Specimens of *C. typicus* were originally isolated from zooplankton samples collected in the Gullmar fjord (Sweden) by vertical tows with plankton nets (500 μ m mesh). Cultures of *C. typicus* were kept in 30 L plastic tanks with sterile-filtered seawater (FSW, salinity 32 ppt), gently aerated, at 16 \pm 1°C in dark. Copepods were fed *ad libitum* with a mix of phytoplankton (the cryptophyte *Rhodomonas sp.*, the diatom *Thalassiosira weissflogii* and the autotrophic dinoflagellates *Heterocapsa triquetra*, *Prorocentrum minimum* and *Gymnodinium sanguineum*) and with the heterotrophic dinoflagellate *Oxyrrhis marina*. Phytoplankton cultures were kept in exponential growth in B1 culture medium and maintained at 18°C and on a 12:12 hr light/dark cycle in glass flasks. *O. marina* was fed the cryptophyte *Rhodomonas salina* and maintained at 18°C in 2 L glass bottles. Behavioural experiments were carried out at room temperature unless otherwise indicated.

Kinematics of startle behaviour

Larvae were relaxed in 50–100 mM MgCl₂ 10 min before tethering them to a Ø3.5 cm glass-bottom dish (HBST-3522, Willco Wells) with a non-toxic glue developed for *C. elegans* (Wormglu, GluStitch Inc). Care was taken to minimize or to avoid gluing ciliary bands, sensory cilia, parapodia, head and pygidium. Prior to the experiment, the glued larvae were assessed for the startle response with a gentle vibration to verify that relevant structures were unhindered, and the animal was healthy and in a swimming mode. 1 μ m multi-fluorescent beads (24062-5, Polysciences) were diluted in 5% BSA to 1:100, sonicated for 1 min and added to the glued larva preparation at a 1:10 dilution. The

experiments were done in a final volume of 2.5 ml. Recordings were done with an AxioZoom V.16 (Carl Zeiss GmbH, Jena) and responses were recorded with a digital CMOS camera ORCA-Flash-4.0 V2 (Hamamatsu). An HXP 200 fluorescence lamp at maximum level (using the Zeiss 45 mCherry filter) was switched on only during each recording (lasting max. 7 s each) to visualize the beads.

To generate water-borne vibrations, a thin 3–5 cm tungsten needle (RS-6063, Roboz) was glued to a shaft-less vibration motor (EXP-R25-390, Pololu), which was switched on for a defined time interval (1–35 ms) and induced the needle to vibrate. The motor was switched on and off with a custom script via an Arduino microcontroller (Arduino UNO R3, Arduino). The probe was positioned in focus at a defined distance from the larva with the manual micromanipulator US-3F (Narishige, Japan). A defined set of stimulation values were used for each of the animals tested, the order of the values was randomized for each larva. Between each stimulation attempt, the larva was left to rest for 1 min. Recordings were discarded if the larva was not in swimming mode while being stimulated. Stimulus start was defined from the videos by the onset of probe movement. The larvae were still alive and visibly healthy one day after being glued. All wild type larvae tested came from different batches. In the case of mutants, 10 larvae from two *PKD1-1^{i1/i1}* batches and 11 larvae from three *PKD2-1^{mut/mut}* batches were tested. Each tested larva was genotyped after the experiment.

The parapodial elevation angle was measured as the movement of the distal end of one of the parapodia in the first segment relative to its base that occurred from the rest position prior to stimulation to the maximal elevation achieved upon stimulation. The value was normalized to the maximum angle recorded for a given larva. Filament speed was calculated as the maximum displacement observed between consecutive frames normalized to the recording speed. Onset of ciliary band closures was defined as the moment after stimulation the flow of fluorescent beads stopped in the vicinity of the cilia. For bodytroch closures this was assessed from the posterior-most band (telotroch). Onset of parapodial elevation was defined as the moment after stimulation when the first segment parapodium (from which the elevation angle was measured) started its angular elevation. The slow elevation speed for LowE responses in many cases made it difficult to assess with precision the start of the elevation movement. The data were analysed with custom R scripts (*Bezares-Calderón, 2018*; copy archived at https://github.com/elifesciences-publications/Bezares_et_al_2018).

Startle assay in freely swimming animals

4 ml of phototactic nectochaete larvae were transferred to a Ø5 cm glass-bottom dish (GWSB-5040, Willco Wells) equipped with a vibrating shaft-less motor glued to its bottom. The motor was activated for 100 ms via an Arduino microcontroller with a custom-written script. The same microscopy equipment was used as for the kinematics experiments, but the recording speed was set to 15 fps. A long-pass filter was placed between the light source and the dish to minimize phototaxis. The speed of startled larvae was calculated as the Pitagorean distance over time unit, and the area was measured from the thresholded shape of the larva.

Whole mount in situ hybridization and immunochemistry

In situ hybridization probes for detecting *PKD1-1* and *PKD2-1* were synthesized from 1 Kb gene fragments subcloned into pCRII vectors (K206001, ThermoFisher) (*Figure 1—figure supplement 1—source data 1*), or from plasmids from an in-house EST library. Whole mount in situ hybridization was done as previously described (*Conzelmann et al., 2011*). The *PKD1-1* and *PKD2-1* promoters (fragment sizes: 2.5 Kb and 1.5 Kb, respectively) were amplified and cloned upstream of 3xHA-Palmi-tdTomato. Larvae injected with promoter constructs (ca. 250 ng/μl) were analysed for reporter expression at 3 days post fertilization using an AxioImager Z.1 fluorescence wide-field microscope (Carl Zeiss GmbH, Jena) and immediately fixed for immunostainings. The protocol followed for immunostaining of HA-tagged reporters was recently described (*Verasztó et al., 2017*). Specimens were imaged with a LSM 780 NLO Confocal Microscope (Zeiss, Jena).

Generation of *PKD1-1* and *PKD2-1* mutants with CRISPR/Cas9

The SpCas9-GFP ORF was kindly provided by Jennifer Doudna (Addgene plasmid #42234) and was subcloned into a custom-made plasmid construct tailored for enhanced mRNA expression in *Platynereis*. sgRNAs were designed using ZiFiT (*Sander et al., 2007*) and cloned into either the DR274 plasmid (kindly provided by Keith Joung, Addgene plasmid #42250) or pX335-U6-Chimeric-BB-CBh-

hSpCas9n (D10A) (kindly provided by Feng Zhang, Addgene plasmid #42335). sgRNAs were synthesized from PCR templates (**Figure 3—figure supplement 1—source data 1**) with the MEGAscript T7 kit (AM1354, Ambion) and purified using the MEGAclear Transcription Clean-up kit (AM1908, Ambion). Zygotes were injected with a mix of 300 ng/μl SpCas9-GFP mRNA and 20 ng/μl sgRNA dissolved in DNase/RNase-free water (10977–049, ThermoFisher). 1-day-old larvae were screened for green fluorescence and gDNA was extracted from single larvae in 4 μl QuickExtract (QE) Solution (QE09050, Epicentre). Mutations were detected by PCR and Sanger sequencing. Adult (atokous) worms injected with effective sgRNAs were genotyped by clipping the pygidium following a previously published protocol (**Bannister et al., 2014**), but using 20 μl of QE solution for gDNA extraction. Worms carrying desired mutations were outcrossed to the wild type strain for the first two generations before using them for experiments.

Phenotyping of mutants

Phototactic nectochaete larvae were transferred to a Petri dish and a single randomly selected larva was placed on a slide in 40 μl fNSW. The larva was scored for the startle response by touching it on the head with a tungsten needle. Only swimming larvae were assayed. For easier interpretation, phenotyped larvae were classified into responders or non-responders. Single larvae were genotyped as described in the preceding section and only after assignment to a phenotype group. The *PKD2-1^{D137}* allele was detectable by gel electrophoresis, and thus only determined by sequencing in ambiguous cases.

Calcium imaging

The *Palmi-3xHA-tdTomato-P2A-GCaMP6s* construct was assembled by restriction cloning from a plasmid kindly provided by Douglas Kim (*GCaMP6s*, Addgene plasmid #40753) and Martin Bayer (*tdTomato*). mRNA was synthesized with the mMACHINE T7 Transcription Kit (AM1344, Ambion). Animals injected with 2 μg/μl mRNA dissolved in RNase-free water were tethered as described for the startle response quantification experiments but using in this case a Ø5 cm glass-bottom dish in 5 ml volume. Tethered larvae were stimulated from the anterior with the filament set at a fixed value that invariably triggered the response. However, the maximum filament speed could not be directly measured for these experiments. Stimulus start was determined from the bright field channel (**Video 4**). In order to minimize muscle contractions, 500 μM Mecamylamine (M9020, Sigma) was added to the dish with the tethered larva. For calcium imaging of muscles no anaesthetic compound was used. Slight X-Y shifts were corrected using descriptor-based series registration (**Preibisch et al., 2010**). Shifts in Z were accounted for with the *tdTomato* signal using the following formula:

$$\Delta R/R = \frac{F(t)_{GCaMP6s} \times F0_{tdTom}}{F0_{GCaMP6s} \times F(t)_{tdTom}}$$

taken from (**Böhm et al., 2016**), where $F0$ is the average fluorescence prior to stimulation calculated from 1/2 the length of the pre-stimulation recorded period. Background signal (non-tissue signal) was used to adjust $F0$ and $F(t)$. Most recordings were done at 4 Hz, 3 recordings at 2.6 Hz.

Circuit reconstruction

CR neurons and the downstream circuit were reconstructed from a ssTEM stack previously reported (**Randel et al., 2015**) using the collaborative annotation tool CATMAID (RRID:SCR_006278; **Saalfeld et al., 2009**; **Schneider-Mizell et al., 2016**). Sensory endings in the left pygidial cirrus could not be imaged and thus CR neurons were not identified there. Chemical synapses were defined as a discrete accumulation of vesicles in the inner side of the presynaptic membrane (**Figure 6—figure supplement 3**). The volume of each synapse was not considered (i.e. each synapse had a weight of 1, independently of how many sections it spanned), and thus the resulting network is a conservative representation of the synaptic strength between neurons. Any given neuron downstream of the CR neurons was included in the analysis if it had three or more synaptic contacts from at least 2 CR neurons. After applying this filter, additional neurons with only 1 or 2 synapses, or only one upstream CR neuron were included if their bilateral counterparts (as defined by neuron morphology) were already part of the first selected set. The targets of the 1st layer in the network were

likewise reconstructed, but only those belonging to the motoneuron class (i.e. cells innervating muscles or ciliary band cells) were included in the circuit. All neurons in the circuit were manually reviewed and weakly connected cells were double checked for accuracy of the synapse annotation. Eight fragments with three or more synapses downstream of the CR neurons but without a cell body were not included in the final circuit. A pair of glial cells, four sensory cells and two interneurons without a bilateral pair were also not included (**Figure 6—source data 1**). The additional penetrating ciliated sensory cells shown in **Figure 6—figure supplement 1** were reconstructed and reviewed only from sensory ending to cell body.

Phylogenetic reconstruction

In addition to PKD1-1 and PKD2-1, a number of homologs to the PKD1 and TRPP families were found in the *Platynereis* transcriptome. A phylogenetic analysis was carried out in order to resolve their relationships. The amino acid sequences of the three human genes in the TRPP family (TRPP2, TRPP3 and TRPP5) and the five homologs of the PKD1 family (PKD1L1-3, PKDREJ and PC1) were used as queries in a BLAST search for homologs against the NCBI nr database. *Platynereis* PKD1 and PKD2 were also used as queries to find additional sequences. Care was taken to collect sequences from animals across the animal phylogeny. Additional sequences were obtained from the COMPAGEN (**Hemrich and Bosch, 2008**), and PlanMine (**Brandl et al., 2016**) databases. Full-length sequences were aligned using Clustal Omega (**Sievers et al., 2011**). For the joint PKD1-PKD2 tree, the alignment was cropped to span only the six transmembrane (TM) domains homologous to the TRP-channel homology region common to both families. For the separate PKD2 and PKD1 family phylogenies any clearly alignable region was included. Only full sequences less than 90% identical were used for the alignment. GBLOCKS alignments (**Talavera and Castresana, 2007**) were used for the phylogenetic reconstruction. Maximum likelihood trees were recovered with PhyML (RRID:SCR_014629; **Guindon et al., 2010**) using the SMS model selection tool (**Lefort et al., 2017**) and aLRT statistics (**Anisimova and Gascuel, 2006**). Sequences were renamed with a custom script (**Bezares-Calderón, 2018**; copy archived at https://github.com/elifesciences-publications/Bezares_et_al_2018).

The GenBank accession numbers of cloned *Platynereis* PKD gene fragments are: PKD2-1, MH035677; PKD2-2, MH035678; PKD1-1, MH035679; LOV-1, MH035680. Full-length sequences from the transcriptome assembly, as well as sequence alignments and the resulting phylogenetic trees are in **Figure 3—figure supplement 1—source data 1**.

SEM of wild type and mutant nectochaete larvae

Mutant and age-matched wild type larvae were collected by phototaxis and simultaneously processed for SEM analysis. In brief, larvae were fixed in 3% Glutaraldehyde/PBS for 3 days (*PKD2-1^{mut/mut}* and its wild type control) or for 1 month (*PKD1-1^{1/1}* and its wild type control) at 4°C. Fixative was then washed out overnight in PBS, and samples were postfixed with 1% OsO₄ for 2 hr on ice. Samples were gradually dehydrated with EtOH and critical point dried following standard protocols. Samples were sputter coated with an 8 nm layer of platinum (Bal-Tec MED010) and imaged with a Hitachi S-800 field emission scanning electron microscope at an accelerating voltage of 15KV. The genotype of fixed larvae was inferred from their sibling larvae.

Predation experiments

Adult stages of male and female *C. typicus* were picked individually from culture bottles and transferred to a beaker with fNSW ca. 2 hr prior to the experiments. The experiments were carried out at 18°C in a Ø7 cm beaker completely wrapped with tin foil (i.e. dark conditions) and filled with 200 ml fNSW. 25 phototactic larvae of each genotype (25 age-matched wild type and 25 *PKD2-1^{mut/mut}*) were transferred to the experimental container and then 5 or 10 copepods were added. Experiments were run for 12 hr or 24 hr without shaking (**Almeda et al., 2017**). At the end of the incubation period, live copepods were counted, and every surviving larva was collected for genotyping. We used 12 mutant batches in 42 experiments (duplicates or triplicates with larvae from the same batch were simultaneously run for a given incubation time). In parallel to each experiment, a negative control with 25 larvae of each genotype but without copepods was run under the same environmental settings to assess mortality not related to predation. In the negative controls, 86% or more larvae

survived, while the maximum survival rate with copepods was 70% (Figure 3—source data 4). Predation rates (I) for each genotype were calculated according to the following formula

$$I = \frac{C_i - C_f}{N \times T}$$

taken from (Almeda et al., 2017), where C_i and C_f are initial and final prey concentrations (prey/L), respectively, N is number of alive predators at the end of experiment and T is incubation time in days. The null hypothesis of equal predation rates was tested against the alternative of a higher predation rate of mutant larvae with a non-parametric one-sided exact Wilcoxon-Pratt signed rank test.

All videos were analysed manually or with custom-written macros in Fiji (RRID:SCR_002285; Schindelin et al., 2012), and data plots were generated in R (RRID:SCR_001905). All panels were assembled into figures using Adobe Illustrator CS6 and CC 2018 (Adobe Systems, Inc.).

Acknowledgments

We thank Ada Kozłowska for help with the initial genotyping of PKD1-1 mutants, Detlev Arendt for providing access to the *Platynereis* genome database, Nadine Randel for fixing samples for SEM, Dorothee Koch and Sinja Mattes for worm culture maintenance, Rocío Rodríguez for copepod culture maintenance and shipments and Elizabeth Williams for comments on the manuscript. The research leading to these results received funding from the European Research Council under the European Union's Seventh Framework Programme (FP7/2007-2013)/European Research Council Grant Agreement 260821. LABC was supported by a grant from the Deutsche Forschungsgemeinschaft (JE 777/3-1). RA was supported by a Marie Curie Intra-European fellowship (6240979) and by the Centre for Ocean Life, a VKR Center of Excellence funded by the VKR Foundation.

Additional information

Funding

Funder	Grant reference number	Author
Deutsche Forschungsgemeinschaft	JE 777/3-1	Luis A Bezares-Calderón
European Commission	260821	Réza Shahidi Gáspár Jékely
European Commission	6240979	Rodrigo Almeda
Max-Planck-Gesellschaft	Open-access funding	Jürgen Berger Sanja Jasek Csaba Verasztó Sara Mendes Martin Gühmann Gáspár Jékely

The funders had no role in study design, data collection and interpretation, or the decision to submit the work for publication.

Author contributions

Luis A Bezares-Calderón, Conceptualization, Resources, Data curation, Software, Formal analysis, Validation, Investigation, Visualization, Methodology, Writing—original draft, Writing—review and editing; Jürgen Berger, Data curation, Visualization, Methodology; Sanja Jasek, Data curation, Formal analysis, Maintenance of catmaid server; Csaba Verasztó, Resources, Data curation, Formal analysis, Connectome tracing; Sara Mendes, Data curation, Visualization, Transgenesis; Martin Gühmann, Resources, Data curation, Formal analysis; Rodrigo Almeda, Resources, Data curation, Formal analysis, Centropages typicus culture; Réza Shahidi, Resources, Data curation, Formal analysis, Visualization; Gáspár Jékely, Conceptualization, Data curation, Formal analysis, Supervision, Funding acquisition, Investigation, Methodology, Writing—original draft, Project administration

Author ORCIDsLuis A Bezares-Calderón  <http://orcid.org/0000-0001-6678-6876>Csaba Verasztó  <http://orcid.org/0000-0001-6295-7148>Martin Gühmann  <http://orcid.org/0000-0002-4330-0754>Gáspár Jékely  <http://orcid.org/0000-0001-8496-9836>**Decision letter and Author response**Decision letter <https://doi.org/10.7554/eLife.36262.055>Author response <https://doi.org/10.7554/eLife.36262.056>**Additional files****Supplementary files**

- Supplementary file 1. Summary of cells that form part of the CR wiring diagram, proposed function and the evidence supporting it.

DOI: <https://doi.org/10.7554/eLife.36262.043>

- Transparent reporting form

DOI: <https://doi.org/10.7554/eLife.36262.044>**Data availability**

Sequencing data have been deposited in Genbank under accession codes MH035677, MH035678, MH035679, MH035680. The neuron reconstructions are available from NeuroMorpho (<https://doi.org/10.13021/degz-cz50>). Code is available at https://github.com/JekelyLab/Bezares_et_al_2018 (copy archived at https://github.com/elifesciences-publications/Bezares_et_al_2018).

The following datasets were generated:

Author(s)	Year	Dataset title	Dataset URL	Database and Identifier
Luis A Bezares-Calderón, Sanja Jasek, Csaba Verasztó, Sara Mendes, Réza Shahidi, Martin Gühmann, Gáspár Jékely	2018	3D reconstructions of neurons in the <i>Platynereis</i> startle circuit	https://doi.org/10.13021/degz-cz50	NeuroMorpho, 10.13021/degz-cz50
Bezares-Calderón LA, Jékely G	2018	Sequencing data	https://www.ncbi.nlm.nih.gov/nuccore/MH035677	Genbank, MH035677
Bezares-Calderón LA, Jékely G	2018	Sequencing data	https://www.ncbi.nlm.nih.gov/nuccore/MH035678	Genbank, MH035678
Bezares-Calderón LA, Jékely G	2018	Sequencing data	https://www.ncbi.nlm.nih.gov/nuccore/MH035679	Genbank, MH035679
Bezares-Calderón LA, Jékely G	2018	Sequencing data	https://www.ncbi.nlm.nih.gov/nuccore/MH035680	Genbank, MH035680

References

- Almeda R, van Someren Gréve H, Kiørboe T. 2017. Behavior is a major determinant of predation risk in zooplankton. *Ecosphere* **8**:e01668. DOI: <https://doi.org/10.1002/ecs2.1668>
- Andersen KH, Berge T, Gonçalves RJ, Hartvig M, Heuschele J, Hylander S, Jacobsen NS, Lindemann C, Martens EA, Neuheimer AB, Olsson K, Palacz A, Prowe AE, Sainmont J, Traving SJ, Visser AW, Wadhwa N, Kiørboe T. 2016. Characteristic sizes of life in the oceans, from bacteria to whales. *Annual Review of Marine Science* **8**: 217–241. DOI: <https://doi.org/10.1146/annurev-marine-122414-034144>, PMID: 26163011
- Anisimova M, Gascuel O. 2006. Approximate likelihood-ratio test for branches: A fast, accurate, and powerful alternative. *Systematic Biology* **55**:539–552. DOI: <https://doi.org/10.1080/10635150600755453>, PMID: 16785212

- Bannister S**, Antonova O, Polo A, Lohs C, Hallay N, Valinciute A, Raible F, Tessmar-Raible K. 2014. TALENs mediate efficient and heritable mutation of endogenous genes in the marine annelid *Platynereis dumerilii*. *Genetics* **197**:77–89. DOI: <https://doi.org/10.1534/genetics.113.161091>, PMID: 24653002
- Barr MM**, Sternberg PW. 1999. A polycystic kidney-disease gene homologue required for male mating behaviour in *C. elegans*. *Nature* **401**:386–389. DOI: <https://doi.org/10.1038/43913>, PMID: 10517638
- Bezares-Calderón LA**. 2018. Bezares_et_al_2018. *GitHub*. 6ef5967. https://github.com/JekelyLab/Bezares_et_al_2018
- Böhm UL**, Prendergast A, Djenoune L, Nunes Figueiredo S, Gomez J, Stokes C, Kaiser S, Suster M, Kawakami K, Charpentier M, Concordet JP, Rio JP, Del Bene F, Wyart C. 2016. CSF-contacting neurons regulate locomotion by relaying mechanical stimuli to spinal circuits. *Nature Communications* **7**:10866. DOI: <https://doi.org/10.1038/ncomms10866>, PMID: 26946992
- Brandl H**, Moon H, Vila-Farré M, Liu SY, Henry I, Rink JC. 2016. PlanMine—a mineable resource of planarian biology and biodiversity. *Nucleic Acids Research* **44**:D764–D773. DOI: <https://doi.org/10.1093/nar/gkv1148>, PMID: 26578570
- Budelmann B-U**. 1989. Hydrodynamic Receptor Systems in Invertebrates. In: Coombs S, Görner P, Münz H (Eds). *The Mechanosensory Lateral Line*. New York, NY: Springer. p. 607–631.
- Bullock TH**. 1984. Comparative Neuroethology of Startle, Rapid Escape, and Giant Fiber-Mediated Responses. In: Eaton R. C (Ed). *Neural Mechanisms of Startle Behavior*. US, Boston: Springer. p. 1–13.
- Calbet A**, Carlotti F, Gaudy R. 2007. The feeding ecology of the copepod *Centropages typicus* (Kröyer). *Progress in Oceanography* **72**:137–150. DOI: <https://doi.org/10.1016/j.pocean.2007.01.003>
- Chalfie M**, Sulston JE, White JG, Southgate E, Thomson JN, Brenner S. 1985. The neural circuit for touch sensitivity in *Caenorhabditis elegans*. *The Journal of Neuroscience* **5**:956–964. DOI: <https://doi.org/10.1523/JNEUROSCI.05-04-00956.1985>, PMID: 3981252
- Conzelmann M**, Offenburger SL, Asadulina A, Keller T, Münch TA, Jékely G. 2011. Neuropeptides regulate swimming depth of *Platynereis* larvae. *PNAS* **108**:E1174–E1183. DOI: <https://doi.org/10.1073/pnas.1109085108>, PMID: 22006315
- Cowles TJ**, Strickier JR. 1983. Characterization of feeding activity patterns in the planktonic copepod *Centropages typicus* Kroyer under various food conditions1. *Limnology and Oceanography* **28**:106–115. DOI: <https://doi.org/10.4319/lo.1983.28.1.0106>
- Eaton RC**, Bombardieri RA, Meyer DL. 1977. The Mauthner-initiated startle response in teleost fish. *The Journal of Experimental Biology* **66**:65–81. PMID: 870603
- Edwards DH**, Heitler WJ, Krasne FB. 1999. Fifty years of a command neuron: the neurobiology of escape behavior in the crayfish. *Trends in Neurosciences* **22**:153–161. DOI: [https://doi.org/10.1016/S0166-2236\(98\)01340-X](https://doi.org/10.1016/S0166-2236(98)01340-X), PMID: 10203852
- Engelmann J**, Hanke W, Mogdans J, Bleckmann H. 2000. Hydrodynamic stimuli and the fish lateral line. *Nature* **408**:51–52. DOI: <https://doi.org/10.1038/35040706>, PMID: 11081502
- Fischer A**, Dorresteijn A. 2004. The polychaete *Platynereis dumerilii* (Annelida): a laboratory animal with spiralian cleavage, lifelong segment proliferation and a mixed benthic/pelagic life cycle. *BioEssays* **26**:314–325. DOI: <https://doi.org/10.1002/bies.10409>, PMID: 14988933
- Fischer AH**, Henrich T, Arendt D. 2010. The normal development of *Platynereis dumerilii* (Nereididae, Annelida). *Frontiers in Zoology* **7**:31. DOI: <https://doi.org/10.1186/1742-9994-7-31>, PMID: 21192805
- Fotowat H**, Fayyazuddin A, Bellen HJ, Gabbiani F. 2009. A novel neuronal pathway for visually guided escape in *Drosophila melanogaster*. *Journal of Neurophysiology* **102**:875–885. DOI: <https://doi.org/10.1152/jn.00073.2009>, PMID: 19474177
- Friesen WO**. 1981. Physiology of water motion detection in the medicinal leech. *The Journal of Experimental Biology* **92**:255–275. PMID: 20968106
- Fritzschn B**, Beisel KW, Pauley S, Soukup G. 2007. Molecular evolution of the vertebrate mechanosensory cell and ear. *The International Journal of Developmental Biology* **51**:663–678. DOI: <https://doi.org/10.1387/ijdb.072367bf>, PMID: 17891725
- Fushiki A**, Zwart MF, Kohsaka H, Fetter RD, Cardona A, Nose A. 2016. A circuit mechanism for the propagation of waves of muscle contraction in *Drosophila*. *eLife* **5**:e13253. DOI: <https://doi.org/10.7554/eLife.13253>, PMID: 26880545
- Guindon S**, Dufayard JF, Lefort V, Anisimova M, Hordijk W, Gascuel O. 2010. New algorithms and methods to estimate maximum-likelihood phylogenies: assessing the performance of PhyML 3.0. *Systematic Biology* **59**:307–321. DOI: <https://doi.org/10.1093/sysbio/syq010>, PMID: 20525638
- Hale ME**, Katz HR, Peek MY, Fremont RT. 2016. Neural circuits that drive startle behavior, with a focus on the Mauthner cells and spiral fiber neurons of fishes. *Journal of Neurogenetics* **30**:89–100. DOI: <https://doi.org/10.1080/01677063.2016.1182526>, PMID: 27302612
- Heckscher ES**, Zarin AA, Faumont S, Clark MQ, Manning L, Fushiki A, Schneider-Mizell CM, Fetter RD, Truman JW, Zwart MF, Landgraf M, Cardona A, Lockery SR, Doe CQ. 2015. Even-Skipped(+) interneurons are core components of a sensorimotor circuit that maintains left-right symmetric muscle contraction amplitude. *Neuron* **88**:314–329. DOI: <https://doi.org/10.1016/j.neuron.2015.09.009>, PMID: 26439528
- Hemmrich G**, Bosch TC. 2008. Compagen, a comparative genomics platform for early branching metazoan animals, reveals early origins of genes regulating stem-cell differentiation. *BioEssays* **30**:1010–1018. DOI: <https://doi.org/10.1002/bies.20813>, PMID: 18800383

- Herberholz J**, Sen MM, Edwards DH. 2004. Escape behavior and escape circuit activation in juvenile crayfish during prey-predator interactions. *Journal of Experimental Biology* **207**:1855–1863. DOI: <https://doi.org/10.1242/jeb.00992>, PMID: 15107440
- Kerfoot WC**. 1978. Combat between predatory copepods and their prey: *Cyclops*, *Epischura*, and *Bosmina* 1. *Limnology and Oceanography* **23**:1089–1102. DOI: <https://doi.org/10.4319/lo.1978.23.6.1089>
- Kjørboe T**, Visser AW. 1999. Predator and prey perception in copepods due to hydromechanical signals. *Marine Ecology Progress Series* **179**:81–95. DOI: <https://doi.org/10.3354/meps179081>
- Knapp MF**, Mill PJ. 1971. The fine structure of ciliated sensory cells in the epidermis of the earthworm *Lumbricus terrestris*. *Tissue and Cell* **3**:623–636. DOI: [https://doi.org/10.1016/S0040-8166\(71\)80009-5](https://doi.org/10.1016/S0040-8166(71)80009-5), PMID: 18631577
- Korn H**, Faber DS. 2005. The Mauthner cell half a century later: a neurobiological model for decision-making? *Neuron* **47**:13–28. DOI: <https://doi.org/10.1016/j.neuron.2005.05.019>, PMID: 15996545
- Kramer AP**, Krasne FB, Wine JJ. 1981. Interneurons between giant axons and motoneurons in crayfish escape circuitry. *Journal of Neurophysiology* **45**:550–573. DOI: <https://doi.org/10.1152/jn.1981.45.3.550>, PMID: 7218014
- Kristan WB**, Calabrese RL, Friesen WO. 2005. Neuronal control of leech behavior. *Progress in Neurobiology* **76**:279–327. DOI: <https://doi.org/10.1016/j.pneurobio.2005.09.004>, PMID: 16260077
- Lacoste AM**, Schoppik D, Robson DN, Haesemeyer M, Portugues R, Li JM, Randlett O, Wee CL, Engert F, Schier AF. 2015. A convergent and essential interneuron pathway for Mauthner-cell-mediated escapes. *Current Biology* **25**:1526–1534. DOI: <https://doi.org/10.1016/j.cub.2015.04.025>, PMID: 25959971
- Lefort V**, Longueville JE, Gascuel O. 2017. SMS: smart model selection in phyML. *Molecular Biology and Evolution* **34**:2422–2424. DOI: <https://doi.org/10.1093/molbev/msx149>, PMID: 28472384
- Lin S**, Staahl BT, Alla RK, Doudna JA. 2014. Enhanced homology-directed human genome engineering by controlled timing of CRISPR/Cas9 delivery. *eLife* **3**:e04766. DOI: <https://doi.org/10.7554/eLife.04766>, PMID: 25497837
- Liu KS**, Fetcho JR. 1999. Laser ablations reveal functional relationships of segmental hindbrain neurons in zebrafish. *Neuron* **23**:325–335. DOI: [https://doi.org/10.1016/S0896-6273\(00\)80783-7](https://doi.org/10.1016/S0896-6273(00)80783-7), PMID: 10399938
- Mackie GO**, Singla CL, Thiriot-Quievreux C. 1976. Nervous control of ciliary activity in gastropod larvae. *The Biological Bulletin* **151**:182–199. DOI: <https://doi.org/10.2307/1540713>, PMID: 963121
- Maguire SM**, Clark CM, Nunnari J, Pirri JK, Alkema MJ. 2011. The *C. elegans* touch response facilitates escape from predacious fungi. *Current Biology* **21**:1326–1330. DOI: <https://doi.org/10.1016/j.cub.2011.06.063>, PMID: 21802299
- Martens EA**, Wadhwa N, Jacobsen NS, Lindemann C, Andersen KH, Visser A. 2015. Size structures sensory hierarchy in ocean life. *Proceedings of the Royal Society B: Biological Sciences* **282**:20151346. DOI: <https://doi.org/10.1098/rspb.2015.1346>
- Nauli SM**, Alenghat FJ, Luo Y, Williams E, Vassilev P, Li X, Elia AE, Lu W, Brown EM, Quinn SJ, Ingber DE, Zhou J. 2003. Polycystins 1 and 2 mediate mechanosensation in the primary cilium of kidney cells. *Nature Genetics* **33**:129–137. DOI: <https://doi.org/10.1038/ng1076>, PMID: 12514735
- Nauli SM**, Kawanabe Y, Kaminski JJ, Pearce WJ, Ingber DE, Zhou J. 2008. Endothelial cilia are fluid shear sensors that regulate calcium signaling and nitric oxide production through polycystin-1. *Circulation* **117**:1161–1171. DOI: <https://doi.org/10.1161/CIRCULATIONAHA.107.710111>, PMID: 18285569
- O’Hagan R**, Chalfie M, Goodman MB. 2005. The MEC-4 DEG/ENaC channel of *Caenorhabditis elegans* touch receptor neurons transduces mechanical signals. *Nature Neuroscience* **8**:43–50. DOI: <https://doi.org/10.1038/nn1362>, PMID: 15580270
- Ohyama T**, Schneider-Mizell CM, Fetter RD, Aleman JV, Franconville R, Rivera-Alba M, Mensh BD, Branson KM, Simpson JH, Truman JW, Cardona A, Zlatic M. 2015. A multilevel multimodal circuit enhances action selection in *Drosophila*. *Nature* **520**:633–639. DOI: <https://doi.org/10.1038/nature14297>, PMID: 25896325
- Pazour GJ**, San Agustin JT, Follit JA, Rosenbaum JL, Witman GB. 2002. Polycystin-2 localizes to kidney cilia and the ciliary level is elevated in orpk mice with polycystic kidney disease. *Current Biology* **12**:R378–R380. DOI: [https://doi.org/10.1016/S0960-9822\(02\)00877-1](https://doi.org/10.1016/S0960-9822(02)00877-1), PMID: 12062067
- Pennington JT**, CHIA FU-S. 1984. Morphological and behavioral defenses of trochophore larvae of *sabellaria cementarium* (polychaeta) against four planktonic predators. *The Biological Bulletin* **167**:168–175. DOI: <https://doi.org/10.2307/1541345>
- Phillips CE**, Friesen WO. 1982. Ultrastructure of the water-movement-sensitive sensilla in the medicinal leech. *Journal of Neurobiology* **13**:473–486. DOI: <https://doi.org/10.1002/neu.480130603>, PMID: 7175520
- Piggott BJ**, Liu J, Feng Z, Wescott SA, Xu XZ. 2011. The neural circuits and synaptic mechanisms underlying motor initiation in *C. elegans*. *Cell* **147**:922–933. DOI: <https://doi.org/10.1016/j.cell.2011.08.053>, PMID: 22078887
- Preibisch S**, Saalfeld S, Schindelin J, Tomancak P. 2010. Software for bead-based registration of selective plane illumination microscopy data. *Nature Methods* **7**:418–419. DOI: <https://doi.org/10.1038/nmeth0610-418>, PMID: 20508634
- Purschke G**. 2005. Sense organs in polychaetes (Annelida). *Hydrobiologia* **535**:53–78.
- Purschke G**, Hugenschütt M, Ohlmeyer L, Meyer H, Weihrauch D. 2017. Structural analysis of the branchiae and dorsal cirri in *Eurythoe complanata* (Annelida, Amphinomida). *Zoomorphology* **136**:1–18. DOI: <https://doi.org/10.1007/s00435-016-0336-5>
- Randel N**, Asadulina A, Bezares-Calderón LA, Veraszó C, Williams EA, Conzelmann M, Shahidi R, Jékely G. 2014. Neuronal connectome of a sensory-motor circuit for visual navigation. *eLife* **3**:e02730. DOI: <https://doi.org/10.7554/eLife.02730>

- Randel N**, Shahidi R, Verasztó C, Bezares-Calderón LA, Schmidt S, Jékely G. 2015. Inter-individual stereotypy of the *Platynereis* larval visual connectome. *eLife* **4**:e08069. DOI: <https://doi.org/10.7554/eLife.08069>, PMID: 26061864
- Roberts A**, Mackie GO. 1980. The giant axon escape system of a hydrozoan medusa, *Aglantha digitale*. *The Journal of Experimental Biology* **84**:303–318. PMID: 6102591
- Ryan K**, Lu Z, Meinertzhagen IA. 2016. The CNS connectome of a tadpole larva of *Ciona intestinalis* (L.) highlights sidedness in the brain of a chordate sibling. *eLife* **5**:e16962. DOI: <https://doi.org/10.7554/eLife.16962>, PMID: 27921996
- Ryan K**, Lu Z, Meinertzhagen IA. 2017. Circuit Homology between Decussating Pathways in the *Ciona* Larval CNS and the Vertebrate Startle-Response Pathway. *Current Biology* **27**:721–728. DOI: <https://doi.org/10.1016/j.cub.2017.01.026>, PMID: 28216318
- Saalfeld S**, Cardona A, Hartenstein V, Tomancak P. 2009. CATMAID: collaborative annotation toolkit for massive amounts of image data. *Bioinformatics* **25**:1984–1986. DOI: <https://doi.org/10.1093/bioinformatics/btp266>, PMID: 19376822
- Sander JD**, Zaback P, Joung JK, Voytas DF, Dobbs D. 2007. Zinc Finger Targeter (ZiFiT): an engineered zinc finger/target site design tool. *Nucleic Acids Research* **35**:W599–W605. DOI: <https://doi.org/10.1093/nar/gkm349>, PMID: 17526515
- Schafer WR**. 2015. Mechanosensory molecules and circuits in *C. elegans*. *Pflügers Archiv - European Journal of Physiology* **467**:39–48. DOI: <https://doi.org/10.1007/s00424-014-1574-3>, PMID: 25053538
- Schindelin J**, Arganda-Carreras I, Frise E, Kaynig V, Longair M, Pietzsch T, Preibisch S, Rueden C, Saalfeld S, Schmid B, Tinevez JY, White DJ, Hartenstein V, Eliceiri K, Tomancak P, Cardona A. 2012. Fiji: an open-source platform for biological-image analysis. *Nature Methods* **9**:676–682. DOI: <https://doi.org/10.1038/nmeth.2019>, PMID: 22743772
- Schlawny A**, Grünig C, Pfannenstiel H-D. 1991. Sensory and secretory cells of *Ophryotrocha puerilis* (Polychaeta). *Zoomorphology* **110**:209–215. DOI: <https://doi.org/10.1007/BF01633005>
- Schneider-Mizell CM**, Gerhard S, Longair M, Kazimiers T, Li F, Zwart MF, Champion A, Midgley FM, Fetter RD, Saalfeld S, Cardona A. 2016. Quantitative neuroanatomy for connectomics in *Drosophila*. *eLife* **5**:e12059. DOI: <https://doi.org/10.7554/eLife.12059>, PMID: 26990779
- Shahidi R**, Williams EA, Conzelmann M, Asadulina A, Verasztó C, Jasek S, Bezares-Calderón LA, Jékely G. 2015. A serial multiplex immunogold labeling method for identifying peptidergic neurons in connectomes. *eLife* **4**:e11147. DOI: <https://doi.org/10.7554/eLife.11147>, PMID: 26670546
- Sharif-Naeini R**, Folgering JH, Bichet D, Duprat F, Lauritzen I, Arhatte M, Jodar M, Dedman A, Chatelain FC, Schulte U, Retailliau K, Loufrani L, Patel A, Sachs F, Delmas P, Peters DJ, Honoré E. 2009. Polycystin-1 and -2 dosage regulates pressure sensing. *Cell* **139**:587–596. DOI: <https://doi.org/10.1016/j.cell.2009.08.045>, PMID: 19879844
- Shaw BK**, Kristan WB. 1995. The whole-body shortening reflex of the medicinal leech: motor pattern, sensory basis, and interneuronal pathways. *Journal of Comparative Physiology A* **177**:667–681. DOI: <https://doi.org/10.1007/BF00187626>, PMID: 8537936
- Sievers F**, Wilm A, Dineen D, Gibson TJ, Karplus K, Li W, Lopez R, McWilliam H, Remmert M, Söding J, Thompson JD, Higgins DG. 2011. Fast, scalable generation of high-quality protein multiple sequence alignments using Clustal Omega. *Molecular Systems Biology* **7**:539. DOI: <https://doi.org/10.1038/msb.2011.75>, PMID: 21988835
- Smith JE**. 1957. The Nervous Anatomy of the Body Segments of Nereid Polychaetes. *Philosophical Transactions of the Royal Society B: Biological Sciences* **240**:135–196. DOI: <https://doi.org/10.1098/rstb.1957.0001>
- Steigleman KA**, Lelli A, Wu X, Gao J, Lin S, Piontek K, Wodarczyk C, Boletta A, Kim H, Qian F, Germino G, Géléoc GS, Holt JR, Zuo J. 2011. Polycystin-1 is required for stereocilia structure but not for mechanotransduction in inner ear hair cells. *Journal of Neuroscience* **31**:12241–12250. DOI: <https://doi.org/10.1523/JNEUROSCI.6531-10.2011>, PMID: 21865467
- Sternberg JR**, Prendergast AE, Brosse L, Cantaut-Belarif Y, Thouvenin O, Orts-Del'Immagine A, Castillo L, Djenoune L, Kurisu S, McDearmid JR, Bardet PL, Boccarda C, Okamoto H, Delmas P, Wyart C. 2018. Pkd2l1 is required for mechanoreception in cerebrospinal fluid-contacting neurons and maintenance of spine curvature. *Nature Communications* **9**. DOI: <https://doi.org/10.1038/s41467-018-06225-x>, PMID: 30228263
- Takagi S**, Cocanougher BT, Niki S, Miyamoto D, Kohsaka H, Kazama H, Fetter RD, Truman JW, Zlatić M, Cardona A, Nose A. 2017. Divergent connectivity of homologous command-like neurons mediates segment-specific touch responses in *Drosophila*. *Neuron* **96**:1373–1387. DOI: <https://doi.org/10.1016/j.neuron.2017.10.030>, PMID: 29198754
- Talavera G**, Castresana J. 2007. Improvement of phylogenies after removing divergent and ambiguously aligned blocks from protein sequence alignments. *Systematic Biology* **56**:564–577. DOI: <https://doi.org/10.1080/10635150701472164>, PMID: 17654362
- Thiel D**, Bauknecht P, Jékely G, Hejnol A. 2017. An ancient FMRFamide-related peptide-receptor pair induces defence behaviour in a brachiopod larva. *Open Biology* **7**:170136. DOI: <https://doi.org/10.1098/rsob.170136>, PMID: 28835571
- Tosches MA**, Bucher D, Vopalensky P, Arendt D. 2014. Melatonin signaling controls circadian swimming behavior in marine zooplankton. *Cell* **159**:46–57. DOI: <https://doi.org/10.1016/j.cell.2014.07.042>, PMID: 25259919
- Verasztó C**, Ueda N, Bezares-Calderón LA, Panzera A, Williams EA, Shahidi R, Jékely G. 2017. Ciliomotor circuitry underlying whole-body coordination of ciliary activity in the *Platynereis* larva. *eLife* **6**:e26000. DOI: <https://doi.org/10.7554/eLife.26000>, PMID: 28508746

- White JG**, Southgate E, Thomson JN, Brenner S. 1986. The structure of the nervous system of the nematode *Caenorhabditis elegans*. *Philosophical Transactions of the Royal Society B: Biological Sciences* **314**:1–340. DOI: <https://doi.org/10.1098/rstb.1986.0056>, PMID: 22462104
- Wiersma CA**, Ikeda K. 1964. Interneurons commanding swimmeret movements in the crayfish, *procambarus clarki* (girard). *Comparative Biochemistry and Physiology* **12**:509–525. DOI: [https://doi.org/10.1016/0010-406X\(64\)90153-7](https://doi.org/10.1016/0010-406X(64)90153-7), PMID: 14206963
- Williams EA**, Jékely G. 2016. Towards a systems-level understanding of development in the marine annelid *Platynereis dumerilii*. *Current Opinion in Genetics & Development* **39**:175–181. DOI: <https://doi.org/10.1016/j.gde.2016.07.005>, PMID: 27501412
- Windoffer R**, Westheide W. 1988. The nervous system of the male *Dinophilus gyrotiliatus* (Annelida: Polychaeta). I. number, types and distribution pattern of sensory cells. *Acta Zoologica* **69**:55–64. DOI: <https://doi.org/10.1111/j.1463-6395.1988.tb00901.x>
- Wine JJ**, Krasne FB. 1972. The organization of escape behaviour in the crayfish. *The Journal of Experimental Biology* **56**:1–18. PMID: 21046844
- Yen J**, Lenz PH, Gassie DV, Hartline DK. 1992. Mechanoreception in marine copepods: electrophysiological studies on the first antennae. *Journal of Plankton Research* **14**:495–512. DOI: <https://doi.org/10.1093/plankt/14.4.495>
- Yoder BK**, Hou X, Guay-Woodford LM. 2002. The polycystic kidney disease proteins, polycystin-1, polycystin-2, polaris, and cystin, are co-localized in renal cilia. *Journal of the American Society of Nephrology* **13**:2508–2516. DOI: <https://doi.org/10.1097/01.ASN.0000029587.47950.25>, PMID: 12239239
- Yoshida S**, Shiratori H, Kuo IY, Kawasumi A, Shinohara K, Nonaka S, Asai Y, Sasaki G, Belo JA, Sasaki H, Nakai J, Dworniczak B, Ehrlich BE, Pennekamp P, Hamada H. 2012. Cilia at the node of mouse embryos sense fluid flow for left-right determination via Pkd2. *Science* **338**:226–231. DOI: <https://doi.org/10.1126/science.1222538>, PMID: 22983710
- Zantke J**, Bannister S, Rajan VB, Raible F, Tessmar-Raible K. 2014. Genetic and genomic tools for the marine annelid *Platynereis dumerilii*. *Genetics* **197**:19–31. DOI: <https://doi.org/10.1534/genetics.112.148254>, PMID: 24807110
- Zhang H**, Yue X, Cheng H, Zhang X, Cai Y, Zou W, Huang G, Cheng L, Ye F, Kang L. 2018. OSM-9 and an amiloride-sensitive channel, but not PKD-2, are involved in mechanosensation in *C. elegans* male ray neurons. *Scientific Reports* **8**:7192. DOI: <https://doi.org/10.1038/s41598-018-25542-1>, PMID: 29740060
- Zucker RS**. 1972. Crayfish escape behavior and central synapses. I. Neural circuit exciting lateral giant fiber. *Journal of Neurophysiology* **35**:599–620. DOI: <https://doi.org/10.1152/jn.1972.35.5.599>, PMID: 5054506